LBL-17681
c.2

Lawrence Berkeley Laboratory
UNIVERSITY OF CALIFORNIA

Materials & Molecular Research Division

RECEIVED
LAWRENCE
BERKELEY LABORATORY
JUL 6 1984
LIBRARY AND
DOCUMENTS SECTION

To be presented at the Second International Symposium on Applications of Laser Anemometry to Fluid Mechanics, Lisbon, Portugal, July 2-4, 1984

DEVELOPING TURBULENT FLOW IN A 180° CURVED PIPE AND ITS DOWNSTREAM TANGENT

J. Azzola and J.A.C. Humphrey

May 1984

TWO-WEEK LOAN COPY
This is a Library Circulating Copy which may be borrowed for two weeks.
~~For a personal retention copy, call Tech. Info. Division, Ext. 6782.~~

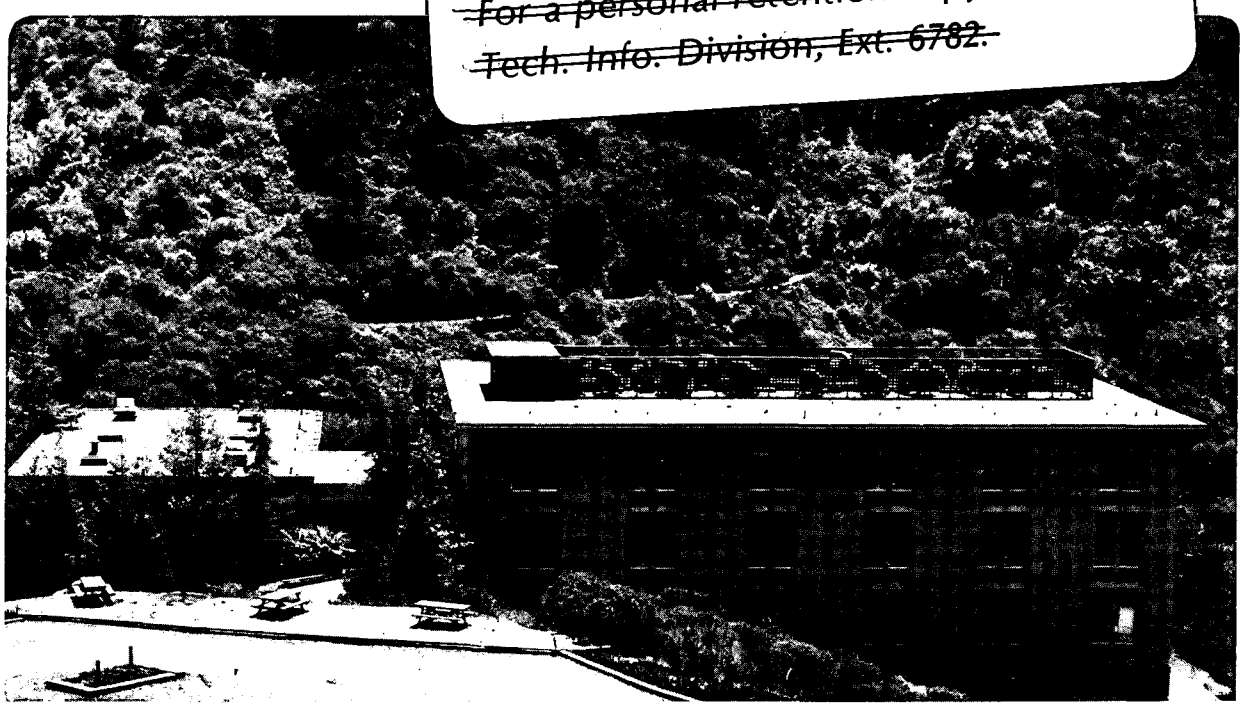

Prepared for the U.S. Department of Energy under Contract DE-AC03-76SF00098

LBL-17681 c.2

DISCLAIMER

This document was prepared as an account of work sponsored by the United States Government. While this document is believed to contain correct information, neither the United States Government nor any agency thereof, nor the Regents of the University of California, nor any of their employees, makes any warranty, express or implied, or assumes any legal responsibility for the accuracy, completeness, or usefulness of any information, apparatus, product, or process disclosed, or represents that its use would not infringe privately owned rights. Reference herein to any specific commercial product, process, or service by its trade name, trademark, manufacturer, or otherwise, does not necessarily constitute or imply its endorsement, recommendation, or favoring by the United States Government or any agency thereof, or the Regents of the University of California. The views and opinions of authors expressed herein do not necessarily state or reflect those of the United States Government or any agency thereof or the Regents of the University of California.

DEVELOPING TURBULENT FLOW IN A 180° CURVED PIPE AND ITS DOWNSTREAM TANGENT

by

J. Azzola[1] and J.A.C. Humphrey[2]

Department of Mechanical Engineering
Lawrence Berkeley Laboratory
University of California
Berkeley, California 94720

LBL-17681

Prepared for presentation at the

SECOND INTERNATIONAL SYMPOSIUM ON APPLICATIONS OF

LASER ANEMOMETRY TO FLUID MECHANICS

July 2 - 4, 1984

Lisbon, Portugal

1. Research Graduate Student
2. Associate Professor

This work was supported through the Office of Fossil Energy of the U.S. Department of Energy under Contract Number DE-AC03-76SF00098 and by the Office of Naval Research through Contract Number N00014-80-C-0031.

CONTENTS

Abstract

Contents

1. Introduction
   1.1 The Problem of Interest and Earlier Work
   1.2 The Present Contribution

2. The Experiment
   2.1 Flow System and Instrumentation
   2.2 Experimental Methodology
   2.3 Measurement Error

3. Results and Discussion
   3.1 The Inlet Flow
   3.2 Mean Flow and Turbulence Intensity
   3.3 Effect of Flow Cross-Section

4. Conclusions

Acknowledgements

References

Tables

Figures

Appendix I: Optical corrections to probe volume location and half angle between beams.

II: Frequency Shifting Procedure

III: Data tabulation.

ABSTRACT

Laser-Doppler measurements of the longitudinal and circumferential velocity components are reported for developing turbulent flow in a strongly curved 180° pipe and its downstream tangent. In the bend, the mean longitudinal velocity component changes little after $\theta = 90°$, but the circumferential component never achieves a fully-developed state. Similar behavior is observed in the normal stresses, with large levels of flow anisotropy arising everywhere in the bend and downstream tangent. Between $\theta = 90°$ and $X/D = 5$, the circumferential velocity profiles display reversals of the secondary flow which are essentially independent of the Reynolds number. Ostensible differences between turbulent flows through pipes of circular and square cross-sections are revealed by comparing present results with the measurements of Chang, et al. [5]. Although limited in extent, the data should serve to guide and test theoretical developments for modeling developing turbulent flows in curved pipes.

1. INTRODUCTION

1.1 The Problem of Interest and Earlier Work

Over the last ten years, approximately, a substantial amount of experimental information has been obtained for developing turbulent flows in curved ducts of rectangular cross-section [1-7]. Detailed measurements in these important flow configurations, in particular of the secondary motions and complex turbulent characteristics which they induce, have been made possible by the non-intrusive laser-Doppler velocimetry technique.

In contrast to the rectangular duct configuration, turbulent flow-field measurements in curved pipes appear to be relatively sparse [8]. This is surprising given the practical importance of the curved pipe configuration. The lack of detailed data is partly explained by the greater difficulty associated with optical alignment of laser beams passing through curved surfaces separating media of different indices of refraction.

Unfortunately, due to the dominant influence of the flat walls on the secondary motion in rectangular ducts, data obtained in these configurations cannot be used to interpret accurately the characteristics of flow developing in curved pipes. For example, in the theoretical analysis by Cuming [9], it is shown that for equal radius of curvature to diameter ratio and dimensionless streamwise pressure drop, the ratio of the relative intensity of the secondary flow in a duct of square cross-section to that in a pipe of circular cross-section is 2.47 at the center line location. This result is strictly valid only for fully developed laminar flow. Comparisons between present results and corresponding

measurements by Chang, et al. [5] in a curved duct of square cross-section with similar developing flow characteristics, show that the secondary motion ratio can be considerably larger than 2.47, depending on the streamwise location. This point will be quantified more precisely in the section on Results and Discussion.

Among the early measurements of secondary turbulent flow patterns developing in and downstream of curved pipes are the total pressure and yaw results obtained by Rowe [10] in a 180° bend. With reference to Fig. 1, the longitudinal stations investigated were θ = 0°, 30°, 60°, 90°, 120°, 150° and 180° in the bend, and X/D = 1, 5, 29 and 61 in the downstream tangent. In Rowe's experiment Rc/D = 12 and Re = 2.36×10^5, where Rc is the bend mean radius of curvature, D its diameter and Re is the Reynolds number based on the bulk fluid velocity. An upstream tangent of length X/D = 69 was used to provide a fully developed axisymmetric turbulent velocity profile at the bend inlet plane. Among Rowe's findings were that: 1) secondary flow is most intense at about θ = 30°, as of which point the total pressure gradient induces a streamwise component of vorticity opposite in sense of rotation to the streamwise vorticity produced at the start of the bend; 2) the curved flow is essentially fully developed past θ = 90°; 3) in the downstream tangent there is a gradual reversion to fully developed turbulent straight pipe flow with the secondary flow persisting past X/D = 29 but being undetectable at X/D = 61; 4) there is evidence of local reversal in the secondary flow direction along the bend symmetry plane between θ = 90° and X/D = 5; 5) the secondary flow appears to be most concentrated at the bend inner radius of curvature; 6) at all longitudinal stations, the

maximum in the streamwise velocity component was always located between the bend center line and the outer radius wall.

Because of the nature of the variables measured in Rowe's study, and because of the influence of the mechanical probes used in the flow, an accurate determination of the fully developed flow streamwise location was not possible. A combination of weak secondary motions, undetected by the yawmeter, with unchanging relatively large total pressure measurements would certainly have given the impression of fully developed flow. Due to experimental uncertainty, Rowe was not able to define precisely the magnitude and extent of secondary flow reversal in the vicinity of the bend symmetry plane. Although valuable for helping to understand the behavior of the mean flow, particularly in relation to inviscid effects, the pressure and yaw contours obtained by Rowe shed no light on the turbulent characteristics of the flow.

In the only laser-velocimetry study known to us for developing turbulent flow in curved pipes, Enayet, et al. [11] investigated the motion in a 90° bend with Rc/D = 2.8 and Re = 43,000. In their study relatively thin boundary layers were induced at the bend inlet plane by means of a smooth contraction. The measurements consisted of longitudinal (streamwise) components of mean and fluctuating velocities only, supplemented by wall-pressure measurements. As expected, the measurements suggest the development of a strong secondary flow in the form of a pair of counter-rotating longitudinal vortices. The secondary flow characteristics were found to depend on the thickness of the inlet boundary layers. In addition, the relatively flat inlet velocity profile and small value of Rc/D in their experiment enhanced streamwise acceleration of the flow at the inner radius wall relative to the outer wall. As a

result, throughout the bend and up to X/D = 6 in the downstream tangent, the peak in the streamwise velocity component remained between the bend center line and the inner radius wall. This finding contrasts strongly with finding (6) of Rowe's study. Because the Dean numbers of these two flows are very similar, being $De = Re\ (D/Rc)^{1/2} \approx 6.8 \times 10^4$ in Rowe's bend and 2.6×10^4 in the bend of Enayet, et al., the difference in the maximum velocity location must be due to the different inlet flow boundary layer thicknesses. A similar finding has been reported in [3] for the flow through a curved duct of square cross section.

In addition to the data taken at three longitudinal stations in the curved pipe, (θ = 30°, 60° and 90°), Enayet, et al. [11] made measurements at X/D = 1 and 6 in the downstream tangent. Although the authors did not measure the cross-stream velocity components at any of these stations, they reported: "a large secondary flow ... now extends over the entire flow area and persists in the plane six diameters downstream of the bend ..." In the absence of secondary component measurements, the inference concerning secondary flow in the downstream tangent could only have been based on the distorted appearance of the streamwise velocity component contours at X/D = 1 and 6, respectively.

1.2 The Present Contribution

The above, admittedly brief, review points to a serious deficiency in the availability of accurate experimental information for illuminating the physics of developing turbulent flow through curved pipes. It is also clear that little seems to be known about the relaxation process undergone by fluid leaving a curved pipe to enter a straight pipe section. The situation is especially serious since for this class of

complex three-dimensional flows such data is indispensable for guiding the development and testing of theoretical models and calculation procedures.

The purpose of this work has been to obtain limited but critical measurements of the longitudinal and circumferential mean velocity components and their respective turbulence intensities at selected longitudinal stations in a 180° curved pipe and its downstream tangent. In addition to its academic significance, this configuration is especially relevant to heat exchangers and particle-laden flow equipment. In the study, special emphasis has been placed on documenting the flow between $\theta = 177°$ in the bend and $X/D = 5$ in the downstream tangent.

2. THE EXPERIMENT

2.1 Flow System and Instrumentation

The experimental system was composed of: a water rig, of which the most important component was the flow test section; a laser-Doppler velocimeter and its associated electronic instrumentation; and a PDP 11/34 Digital Equipment Corporation minicomputer.

The basic components of the flow test section are shown schematically in Fig. 1. They comprised two straight pipes and a 180° curved pipe, constructed from transparent plexiglass. The pipe cross-section was circular throughout with a 4.45 cm ± 0.02 cm inner diameter (D). The ratio of bend mean radius of curvature (Rc) to pipe diameter was $Rc/D = 3.375$. Both tangents were of length $x = 54.7$ D, being respectively attached to the 0° (inlet) and 180° (outlet) planes of the bend by means of flanges. Special care was taken to avoid possible mismatches between the component cross-sections which otherwise might disturb the

flow. A stainless steel (20 mesh) screen and a 3.5 cm long flow straightening honeycomb section were placed upstream of the entrance tangent. They were held in place by a thin plexiglass plate. The plate was 3.175 mm thick and had 85 holes of 3.175 mm diameter arranged in a rectangular array spaced 4.495 mm on the centers in each direction. The purpose of the screen-honeycomb-plate combination was to make uniform the cross-stream plane distribution of the flow and accelerate its streamwise development.

The curved pipe section was constructed by fitting together two symmetrical half sections of plexiglass, each respectively machined on one of its flat faces to contain the shape of a semicircular open channel. This method of construction ensured that when matched at the common symmetry plane the cross-section of the resulting curved pipe was accurately circular. When assembled, the curved pipe section had flat outer surfaces of thickness $d = 1.48 \pm 0.02$ cm (see Fig. 1). The straight pipe sections had a circumferentially uniform wall thickness of 0.32 ± 0.02 cm. The entire test section was supported horizontally by a unistruct structure, with the bend symmetry plane parallel to the floor.

The test section was part of a closed loop through which water was made to flow by gravity from a constant head tank. From this tank the flow passed through the test section, and then into a large sump tank from where it was pumped back to the constant head tank. Flow to the head tank was controlled by a gate valve and measured using a venturi meter connected to a differential mercury manometer. The possibility of propagating disturbances through the test section was eliminated by avoiding the use of valves, sharp bends and metering devices in the test section flow loop. Flow to and from the test section tangents was chan-

neled through 2 in (5.08 cm) i.d. gently bent tygon tube pieces. Baffles and screens located in the constant head tank served to dampen the swirling motion of the flow leaving the tank. Residual swirl and weak secondary motions induced by the mild curvature in the tygon tube upstream of the test section were eliminated by the flow straightening section.

Measurements of the mean flow and turbulence characteristics were made using a DISA 55X modular series laser-Doppler velocimeter in backscatter mode. The system has already been described in full detail in reference [5]. A 2-watt Lexel Argon-Ion water-cooled laser was used as the light source. The laser and velocimeter optics were mounted to the top of a thick aluminum table which was itself firmly bolted to an x, y, z traversing mechanism. The traversing mechanism could displace the table top ± 7.5 cm in 5 μm increments along any of the coordinate axes by means of three linearly encoded stepping motors monitored by the PDP 11/34 minicomputer. The minicomputer functioned as the central data acquisition and reduction controller of data validated and measured by a DISA 55L96 Doppler signal procesor or "counter." Directional ambiguity in the circumferential (or tangential) velocity component was resolved by means of a Bragg cell combined with electronic downmixing.

2.2 Experimental Methodology

Prior to an experimental run, water was allowed to flow through the rig until it was purged of air bubbles and had attained a steady thermal state corresponding to about 20°C. Mass flow through the test section was controlled by setting the constant head overflow condition to a mere trickle and continuously monitoring the pressure drop through the venturi

meter connected to the head tank feed line. Experiments were performed for two values of the bulk average velocity corresponding to $U_b = 1.29 \pm 0.03$ m/s and $U_b = 2.47 \pm 0.04$ m/s, respectively. During the course of an experimental run the fluid temperature rose from 18°C to 22°C, approximately. Values for the Reynolds numbers of these two flows, based on physical properties of water at 20°C, are Re = 57,400 and 110,000, respectively. The associated Dean numbers are De = 31,300 and 59,900.

The velocimeter optical probe volume was formed by the intersection of two 514.5 nm (green) light beams with a half-angle in air of 3.28°. The measurement volume charateristics were: a diameter of 0.1 mm, a length of 1.6 mm, and a fringe spacing of 4.50 μm with about 18 fringes contained in the optical probe. In reality spatial filtering and threshold settings on the counter reduced the dimensions of the optical probe. The probe volume was positioned by fine control of the motorized traversing table.

At each measurement station initial positioning of the laser beams with respect to the plexiglass surface was achieved through the use of reference markers. Paper drawn with precise cross hairs was taped onto the flat outer surface of the curved pipe section and the beams were aligned with respect to the marks, checking that no sideways beam deviation occurred as the beams were displaced in the vertical direction. After the paper was removed, symmetrical reflections facilitated vertical alignment of the optical volume in the cross-stream plane. Alignment of the beams in the straight pipe sections was performed in a similar manner. Special care was taken to ensure that the optical probe fringe pattern was always aligned normal to the velocity component of interest to within ± 0.3°.

With a reference position established, usually on the outer surface of the test section, the computer software was activated which controls signal acquisition and data processing. An initial check on flow symmetry was performed at X/D = -2 in the upstream tangent. Measurements of the streamwise velocity component and its normal stress at this station (half profiles are shown in Figs. 2 and 4) are in good agreement with the data of Laufer [19]. Measurements of the circumferential velocity component (not plotted) showed that it was everywhere less than ~ 1.5% of the bulk average velocity at this station. Calculations of U_b, obtained by integrating the measured velocity distributions at X/D = -2, yielded values in good agreement (to within ~ 3%) with the values obtained from the venturi meter pressure drop readings.

Following the symmetry and mass flow confirmations, all subsequent measurements were restricted to vertical (radial) scans in the plane $\phi = \pi/2$ in the symmetrical upper half of the test section. Scans were made at X/D = -2, -1, 1, 2, 3, 4 and 5 in the straight pipes and θ = 30°, 45°, 90°, 135°, and 177° in the bend. At each of these stations 15 radial positions were probed, starting at the centerline and moving in increments of 1.5 mm toward the wall, with a 16th position fixed at 0.73 mm from the inside pipe wall. At each measurement point the mean flow and turbulence characteristics were statistically determined from populations of 1 to 3 samples consisting of 1,000 individual measurements each. More than 90% of all the measurements consisted of at least 2 samples per point. Each individual measurement was required to satisfy the counter 5/8 validation comparison to within a preset tolerance of 6%. At every validation of a Doppler burst a "data ready" signal was issued by the counter to a logic conversion circuit. This circuit then sent a

triggering pulse to the computer parallel line interface module which was checked for data availability by a software loop approximately every 20 μs.

Attempts were made to optimize signal quality and particle concentration. Corn starch, with particles ranging in size between 1 and 10 μm, was found to give a consistently high signal-to-noise ratio in addition to a low settling rate. Alternative particle types rejected include TiO_2, non-dairy creamers, and mother-of-pearl. Data rates varied from 50-1000 Hz, with counter validation levels ranging between 10 and 90% approximately. Factors influencing these levels included, in order of relative importance: optical alignment, thickness of the wall, probe volume location in the flow field, and seeding concentration.

Although the velocimeter is capable of two-component measurements, curvature of the test section surfaces precluded dual-channel operation. Values for the streamwise component of the mean and fluctuating velocities, U and u', were derived from measurements obtained with the probe volume fringes aligned normal to the longitudinal coordinate direction. Values for the circumferential components, V and v', were obtained through a rotation of the optics by 90°, thus placing the fringes normal to the circumferential component direction.

Because of the large positive magnitudes of the streamwise velocity component, frequency shifting was unnecessary for measurements of this component. By contrast, the circumferential velocity component exhibited low magnitudes, with signs both positive and negative. To resolve this directional ambiguity, a net frequency shift of 500 kHz was imposed using a DISA 55N10 Bragg cell combined with electronic downmixing. Appendix II provides an explanation for implementing the frequency shift procedure.

2.3 Measurement Error

Error sources affecting the accuracy (systematic error) and precision (random error) of laser-Doppler measurements have been discussed by, for example, Durst, et al. [12], Drain [13] and Buchhave [14]. In this study the most serious potential systematic errors were attributed to probe volume positioning, velocity gradient broadening and velocity bias, respectively. The main sources of random error affecting the precision of the measurements were due to: a) statistical sampling uncertainty (due to the finite size of sample populations); and b) uncertainty in the determination of the normalizing bulk average velocity, U_b. Estimates of the first uncertainty were derived from the measurements themselves. For both mean velocity components, this uncertainty was always less than ± 2-3% (r.m.s. error), while for the turbulence intensities it was always less than ± 2-5%. The error in U_b was ± 2% and arose principally from uncertainities in the manometer pressure readings.

The initial probe volume location uncertainty was estimated to be half the effective probe volume length, or ± 0.5 mm approximately. This error is altered as the beams traverse the pipe because of index of refraction and wall curvature effects. To calculate the actual probe volume location, and to estimate the uncertainty in this location, it is necessary to know the relevant trigonometric relations. Two of the three cases of interest here have been analyzed by Bicen [15] and Boadway and Karahan [16], respectively. The present authors have found inconsistencies in the analyses in these references, as well as between them for identical configurations. For this reason it was considered prudent to rederive the trigonometric relations of relevance to this study. Appendix I presents relations corresponding to flows bounded by: a)

parallel flat surfaces; b) concentric cylindrical surfaces; and, c) one flat and one cylindrical surface.

For parallel and concentric cylindrical surfaces, references [15-16] obtained:

$$U = C_f U_M$$

In this relation U_M is the velocity measurement obtained in, for example, water using a half angle between beams in, for example, air. The factor C_f is necessary to "correct" the measurement so that the result represents the water velocity. For parallel surfaces, to a small angle approximation it can be shown that:

$$U = (\alpha/\gamma) U_M = \eta_f U_M$$

where: α is the beam half angle in air, γ is the beam half angle in water, and η_f is the index of refraction of water relative to air (here taken as 1.333). Curiously, reference [15] takes $C_f = 1$ for parallel surfaces, a result valid only for air as the working fluid. Similarly, the expression in [16] for C_f for correcting circumferential velocity measurements is in error by a factor of η_f.

Table 1 summarizes the relations derived for the various cases analyzed in Appendix I. The relations depend on the velocity component of interest and the shape of the surfaces at the measurement station in question. For example, the beam orientation required to measure the longitudinal velocity component in the plane $\phi = \pi/2$ renders the beams insensitive to surface curvature effects. For this component the beams are crossed such that their bisector is normal to the test section surface and the beams are contained in the $\phi = \pi/2$ plane. Therefore, for

all practical purposes, both in the curved and straight pipe sections the beams behave as if they were passing through a pair of parallel interfaces[1]. By contrast the orientation required to measure the circumferential velocity component makes it necessary to distinguish between the straight and curved pipe sections. For this component the beams are crossed such that their bisector is normal to the test section surface and is contained in the $\phi = \pi/2$ plane, while the beams themselves are contained in a plane perpendicular to the $\phi = \pi/2$ plane.

Table 1 shows that in regions of surface curvature, both the probe volume location and the half angle between the beams in water depend nonlinearly on the probe volume virtual radial location (the location in air). Calculations of the error incurred in γ, the half angle of the beams in water, due to a ± 0.5 mm positioning error in the initial probe volume location showed that this source of inaccuracy was negligible. Similarly, calculations showed that the initial positioning uncertainty was only significant very near the pipe walls, in regions with steep gradients. Thus, estimates of the maximum (absolute) systematic errors in the measurements obtained nearest the walls gave: ~ 4% for U/U_b; ~ 10% for u'/U_b; ~ 15% for V/U_b, and ~ 10% for v'/U_b. In the bulk of the flow all these errors were significantly less than ~ 2%.

Velocity gradient broadening has been analyzed by Melling [18] who proposed a simple method for estimating its magnitude. For the con-

****

[1] Due to the small angle between the beams, the error incurred in the bend as a consequence of making this approximation is negligible.

ditions of this study, gradient broadening in the measurements was estimated to be less than 1% everywhere in the flow.

Various weighting methods have been proposed to correct for the velocity bias effect [13,14], but none of these is entirely satisfactory. They all involve assumptions regarding the statistical distribution of particles in the flow. In addition, the corrections can be influenced by the problem of "incomplete-signal bias." The use of the weighting scheme proposed by McLaughlin and Tiederman [17], in which the particle residence time is taken to be inversely proportional to the modulus of the measured velocity, was investigated in this study. For the longitudinal velocity component, differences between weighted and unweighted data sets were relatively small (less than 1%). For the circumferential component the differences were much larger, with the weighted data giving a less realistic (overdamped) picture of the flow field. The reason for this is attributed to an overcorrection in the weighting scheme which, for the circumferential component, amounts to a disproportionate weighting of slow moving particles. This occurs as a consequence of taking the particle residence time as $t_{res} \sim V^{-1}$ instead of $t_{res} \sim (U^2 + V^2 + W^2)^{-1/2}$. The latter, more accurate, weighting could not be performed with the present single component measurement system.

For turbulence intensities less than 10% Drain [13] shows that velocity bias corrections of the mean and r.m.s. velocities should not amount to more than ~ 2%. In this study the measured turbulence intensities never exceed ~ 12%. As a result, plots of the unweighted data only are presented here. Appendix III contains a listing of both the weighted and unweighted measurements.

3. RESULTS AND DISCUSSION

Measurements of the longitudinal (U/U_b) and circumferential (V/U_b) velocity components and their respective turbulence intensities (u'/U_b, v'/U_b) are shown in Figs. 2-5 and are tabulated in Appendix III. Except for relatively small differences, the dimensionless profiles show that flow development is essentially independent of Reynolds number for $Re > 57{,}400$.

3.1 The Inlet Flow

The U and u' component measurements at X/D = -2 show good agreement with the developed flow measurements obtained by Laufer [19] in a straight pipe. At X/D = -2 the V component is less than (+) 0.015 U_b (not plotted). However, at X/D -1 and $\theta = 3°$, the V component is ~ (+) 0.04 U_b. With reference to the coordinate system in Fig. 1, this implies that the inlet flow is gradually (but only slightly) accelerated towards the inner radius of the pipe, a result expected from potential flow theory and previously observed by others.

3.2 Mean Flow and Turbulence Intensity

In the first half of the bend ($\theta = 3°$ to $90°$), the U-profiles show the core of the streamwise flow losing speed while the flow near the wall accelerates. V-profiles at corresponding stations reveal the development of a strong secondary flow. This secondary flow is induced by the transverse pressure gradient set up between the outer (r_o) and inner (r_i) wall regions of the bend. In the pipe center, it works to overcome and reverse the sense of the cross-stream motion in the inlet flow. Near the

wall the original sense of cross-stream motion is preserved and intensified, with $(V/U_b)_{max} \sim 0.30$ at $\theta = 45°$.

Between $\theta = 45°$ and 135° the V-profiles reveal a striking feature of the flow. In the fluid core, $r/(D/2) < 0.5$, the cross-stream flow undergoes a <u>second reversal</u> in its sense of motion and is redirected towards the pipe inner radius. As a result, a region of negative cross-stream flow (directed from r_i towards r_o) is trapped between the core and the wall; for example, $V/U_b \sim -0.06$ at $\theta = 135°$. Between $\theta = 135°$ in the bend and $X/D = 5$ in the downstream tangent, the region of negative cross-stream flow gradually disappears. Notwithstanding, an imprint of its presence remains in all the V-profiles.

The occurrence of a second cross-stream flow reversal past $\theta = 90°$ in the bend supports the concept proposed by Rowe [10], that each symmetrical half section of the bend develops <u>two</u> counter-rotating vortical structures. The more intense of the two, located between the pipe wall and the core of the flow, preserves the sense of cross-stream motion induced by the transverse pressure gradient at the start of the bend. The smaller, weaker, structure is mainly confined to the core and is attributed to the formation of a transverse pressure gradient opposite in sign to that at the start of the bend.

The present mean flow measurements place on a firm quantitative basis the interpretation by Rowe of his total pressure and yaw measurements. However, in contrast to Rowe's results, the V-profiles provided here show that fully developed mean flow conditions are not established in the bend.

There is a qualitative similarity between the present V-profiles and corresponding laminar flow measurements made by Olson and Snyder [20] in

300° curved pipes. In their experiments two curvature ratios (Rc/D = 2.33 and 8) were investigated for two values of the Reynolds number (Re = 300 and 1030). The inlet flow was contracted to produce nearly flat entrance profiles. Measurements of the cross-stream flow were made at several longitudinal stations with a pulsed-probe anemometer. Between θ = 40° and 90° the authors found a cross-stream flow reversal in the center of the pipe similar to the present one.

The longitudinal variation of the local ratio V/U is plotted in Fig. 6 for two values of $r/(D/2)$ in the present flow. The profiles show clearly the cross-stream flow reversals which arise in the bend. They also show that, although substantially reduced, secondary motion persists between θ = 177° and X/D = 5 in the downstream tangent, and is stronger near the pipe center than at the wall.

Figure 6 also summarizes the most interesting variations of the turbulence components u'/U_b and v'/U_b in the bend and downstream tangent. Actually plotted is the ratio v'/u', a measure of turbulent flow anisotropy. Because the data are relatively few and restricted to the $\phi = \pi/2$ plane shown in Fig. 1, and because the physical processes governing the generation, redistribution and destruction of the turbulent stresses are complex, it is not possible to render more than a speculative account of the meaning of our measurements. Bearing this in mind, we note that near the wall, $r/(D/2)$ = 0.75, the ratio v'/u' increases persistently between X/D = -1 and θ = 90°. Because this coincides with a correspondingly large increase in V, we suspect that the term $-\overline{vw}\,\partial V/\partial r$ contributes strongly to the generation of v'^2 ($\equiv \overline{v^2}$) near the wall. As of θ = 90° the ratio v'/u' decreases near the wall. The decrease is due to a gradual reduction in v' (as opposed to an increase in u') as the

flow evolves; see Figs. 2 and 3. Because $\partial V/\partial r$ peaks at about $\theta = 45°$, from this position forward we argue that $-\overline{vw}\,\partial V/\partial r$ now contributes decreasingly to the balance of v'^2. This then allows dissipation and redistribution mechanisms to reduce the level of v'^2 near the wall, as observed.

The core flow, $r/D(2) = 0$, experiences a marked decrease in v'/u' between $\theta = 45°$ and $90°$ in the bend. Between these locations the quantity $\partial V/\partial\theta$ is large and positive. Inspection of the data for $\overline{uv}$ obtained by Chang, et al. [5] in a curved duct of square cross-section suggests that in the core of the present flow $\overline{uv}$ is positive. As a result, the term $-\overline{uv}\,\partial V/\partial\theta$ should be expected to contribute <u>negatively</u> to the balance of v'^2 (and hence reduce this component) between $\theta = 45°$ and $90°$.

The increase in v'/u' between $\theta = 90°$ and $X/D = 1$ in the core of the flow is more difficult to explain. It is probably related to the convection of v'^2 from the wall periphery (where v'^2 is generated) into the core.

The ratio v'/u' in the flow entering the bend at $X/D = -1$ is in qualitative agreement with Laufer's [19] pipe flow data, both at $r/(D/2) = 0$ and 0.75. In the downstream tangent the expected level of v'/u' is re-established near the pipe wall within 5 pipe diameters. By contrast, the turbulence remains strongly anisotropic in the core of the flow. The persistence of this anisotropy may be related to the presence of an extra pair of symmetrical vortical structures, discussed earlier in relation to cross-stream flow reversal.

3.3 Effect of Flow Cross-Section

A comparison was made between some of the present results for Re = 57,400 and corresponding measurements obtained by Chang, et al. [5] in a 180° curved duct of square cross-section with Rc/D = 3.35 and Re = 56,700. Plots of square(s)-to-round(r) ratios of circumferential mean velocities and corresponding turbulence intensities are shown in Fig. 7.

Absolute values of $[V/U_b]_s/[V/U_b]_r$ considerably larger than unity illustrate clearly the dominant influence exercised by the flat walls on most of the flow through a curved square duct. (Negative values in the plots are due to the cross-stream flow reversal occurring in the pipe but not in the duct.)

At X/D = -1 the inviscid transverse motion induced through longitudinal curvature in the pipe was found to be twice as strong as that in the duct. However, because the Re and Rc/D ratios between the two configurations is so close, potential flow theory would predict essentially equal cross-stream flow. Therefore, we conclude that: a) the more intense secondary motion subsequently induced in the duct (due to the transverse pressure gradient) acts to suppress the initial inviscid component of transverse flow; and, b) this effect reaches further upstream into the straight duct than into the straight pipe.

The circumferential turbulence intensity ratios plotted in Fig. 7 show larger fluctuation levels near the flat wall of a curved duct than near the side wall of a curved pipe. This is in keeping with the higher velocities and hence higher rates of shear expected along the flat walls of a curved duct. Surprisingly, in the core of the flow the fluctuations are always larger in the pipe and may be related to the additional pair

of symmetrical counter-rotating vortices which develop in the core of the curved pipe. The relatively large value of $[v'/U_b]_s/[v'/U_b]_r$ shown at X/D = -1, near the wall, is attributed to corner contributions to fluctuations, present only in the square duct.

4. CONCLUSIONS

This study places on a firm quantitative basis some of the earlier qualitative interpretations proposed by Rowe [10] for the mean behavior of turbulent flow through a 180° curved pipe. Specifically, the existence of two cross-stream flow reversals is confirmed. This supports the notion of an additional (symmetrical) pair of counter-rotating vortical structures embedded in the core of the flow within the curved pipe and part of the downstream tangent. Fully developed flow conditions are never attained in the present bend.

Interpretation of our measurements points to strong generation of circumferential fluctuations along the pipe periphery due to the main secondary flow. By contrast, negative contributions to generation dampen circumferential fluctuations in the core. It is argued that the dampening is offset by cross-stream convection of v'^2 from the bend periphery into the core of the flow.

A comparison between the cross-stream motions in curved circular pipes and curved square ducts shows that the latter have considerably higher levels of secondary flow. Cross-stream flow reversals were not observed in the square duct configuration. It is suggested that the larger relative levels of cross-stream fluctuations detected in the core

of a curved pipe flow are probably related to the presence there of an additional pair of symmetrical counter-rotating vortices.

Continued work should focus on extending the data base for clarifying the role of the additional pair of vortical structures in curved pipe flow and the relaxation process occurring in the downstream tangent.

ACKNOWLEDGEMENTS

This study is the result of a continuing collaboration between one of the present authors (JACH) and Professor Brian E. Launder at the University of Manchester, Institute of Science and Technology. The collaboration aims to further the understanding of turbulent flow convective heat transfer in strongly curved passages. The work at the University of California, Berkeley, was initially supported by the Office of Naval Research through Contract Number N 00014-80-C-0031 and, more recently, by the Office of Fossil Energy of the U.S. Department of Energy under Contract Number DE-AC03-76SF00098. We are grateful to these agencies for their respective support. Thanks go to Ms. Loris C-H Donahue for the typing of this manuscript.

REFERENCES

1. Humphrey, J.A.C., Whitelaw, J.H. and Yee, G. "Turbulent flow in a square duct with strong curvature," J. Fluid Mech., 103, pp. 443-463, 1981.

2. Enayet, M.M., Gibson, M.M. and Yianneskis, M. "Measurements of turbulent developing flow in a moderately curved square duct," Int. J. Heat and Fluid Flow, 3, No. 4, pp. 221-224, 1982.

3. Taylor, A.M.K.P., Whitelaw, J.H. and Yianneskis, M. "Curved ducts with strong secondary motion: velocity measurements of developing laminar and turbulent flow," J. Fluids Engng., 104, pp. 350-359, 1982.

4. Anderson, B.H., Taylor, A.M.K.P., Whitelaw, J.H. and Yianneskis, M. "Developing flow in S-shaped ducts," Proc. Int. Symposium on Applications of Laser-Doppler Anemometry to Fluid Mechanics, Lisbon, July 1982.

5. Chang, S.M., Humphrey, J.A.C. and Modavi, A. "Turbulent flow in a strongly curved U-bend and downstream tangent of square cross-sections," PhysicoChemical Hydrodynamics, 4, No. 3, pp. 243-269, 1983.

6. Rojas, J., Whitelaw, J.H. and Yianneskis, M. "Flow in sigmoid diffusers of moderate curvature," Proc. Fourth Symposium on Turbulent Shear Flows, Karlsruhe, FDR, September 1983.

7. Brunn, H.H., "An experimental investigation of secondary flow losses in bends with rectangular cross sections," Department of Engineering, Report CUED/A-Turbo/TR 95, University of Cambridge, 1979.

8. Berger, S., Talbot, L. and Yao, L.-S. "Flow in curved pipes," Ann. Rev. Fluid Mech., 15, pp. 461-512, 1983.

9. Cuming, H.G. "The secondary flow in curved pipes," Reports and Memoranda, No. 2880, February 1952.

10. Rowe, M. "Measurements and computations of flow in pipe bends," J. Fluid Mech., 43, pp. 771-783, 1970.

11. Enayet, M.M., Gibson, M.M., Taylor, A.M.K.P. and Yianneskis, M. "Laser-Doppler measurements of laminar and turbulent flow in a pipe bend," Int. J. Heat and Fluid Flow, 3, pp. 211-217, 1982.

12. Durst, F., Melling, A. and Whitelaw, J.H. "Principles and Practice of laser-Doppler Anemometry," Academic Press, London, 1976.

13. Drain, L.E. "The Laser Doppler Technique," John Wiley and Sons Ltd., New York, 1980.

14. Buchave, P. "The measurement of turbulence with the Burst-type laser-Doppler Anemometer - Errors and Correction Methods," Ph.D. Thesis, State University of New York at Buffalo, 1979.

15. Bicen, A.F., "Refraction correction for LDA measurements in flows with curved optical boundaries," Report FS/81/17, Department of Mechanical Engineering, Imperial College of Science and Technology, London University, 1981.

16. Boadway, J.D. and Karahan, E. "Correction of laser-Doppler anemometer readings for refraction at cylinderical interfaces," DISA Information, No. 26, pp. 4-6, 1981.

17. McLaughlin, D.K. and Tiederman, W.G. "Biasing correction for individual realization of laser anemometer measurements in turbulent flows," Physics of Fluids, 16, pp. 2082-2088, 1973.

18. Melling, A. "Investigation of flow in non-circular ducts and other configurations by laser-Doppler anemometry," Ph.D. Thesis, University of London, 1975.

19. Laufer, J. "The Structure of Turbulence in Fully Developed Pipe Flows," NACA Technical Reports No. 1174, 1954.

20. Olson, D.E. and Snyder, B. "The Growth of Swirl in Curved Circular Pipes," Phys. Fluids, 26 (2), pp. 347-349, 1983.

TABLE 1: SUMMARY OF BEAM CORRECTION FORMULAE

Configuration	Position (r_v/r) and Velocity (α/γ) Factors
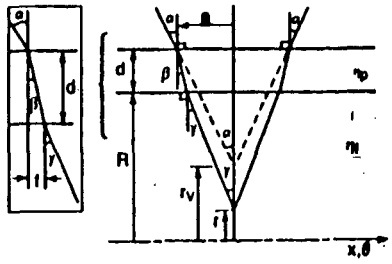	$\frac{r_v}{r} = \frac{1}{\eta_f} + \frac{R}{r}\,\frac{\eta_f - 1}{\eta_f} + \frac{d}{r}\,\frac{\eta_p - 1}{\eta_p}$
	$\frac{U}{U_M} = \frac{\alpha}{\gamma} = \eta_f$
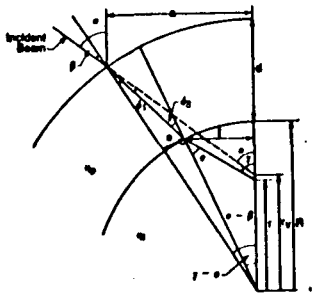	$\frac{r_v}{r} = \frac{\eta_f}{1 - \frac{r\,\eta_f}{R + d}\left(\frac{R + d}{R\,\eta_f} - 1 - \frac{d}{R\,\eta_p}\right)}$
	$\frac{V}{V_M} = \frac{\alpha}{\gamma} = \frac{1}{1 + \frac{r_v}{R + d}\left[\frac{R + d}{R\,\eta_f} - 1 - \frac{d}{R\,\eta_p}\right]}$
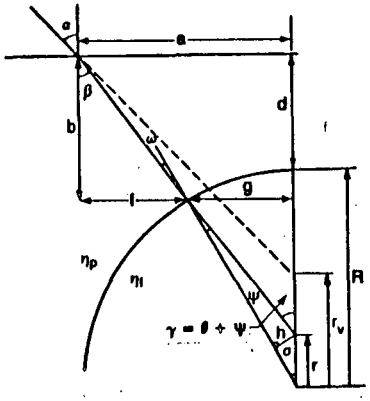	$\frac{r_v}{r} = \frac{R\left[\frac{R}{r}\left(1 + \frac{d}{R}\right)\frac{\eta_p - 1}{\eta_f} + 1 + \frac{d}{R}\left(\frac{\eta_p - 1}{\eta_p} - \frac{\eta_p - 1}{\eta_f}\right) - \frac{\eta_p - 1}{\eta_f}\right]}{r\,\frac{\eta_f - \eta_p}{\eta_f} + R\,\frac{\eta_p}{\eta_f}}$
	$\frac{V}{V_M} = \frac{\alpha}{\gamma} = \frac{1}{1 - \frac{\eta_p - 1}{\eta_f} + \frac{r_v}{R}\,\frac{\eta_p - \eta_f}{\eta_f} + \frac{d}{R}\left(\frac{\eta_p - 1}{\eta_p} - \frac{\eta_p - 1}{\eta_f}\right)}$

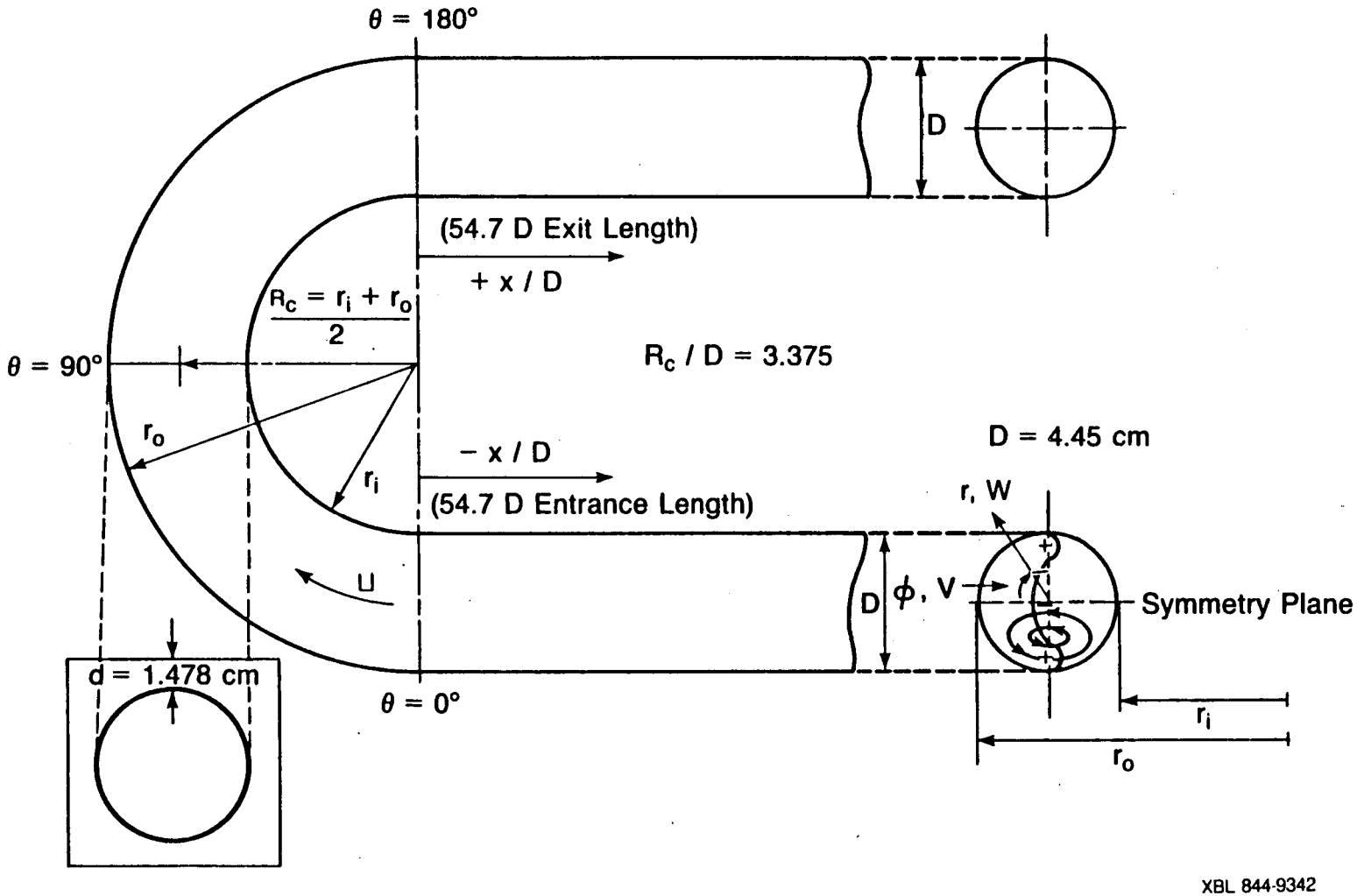

Figure 1. The test section configuration and definition of coordinate system.

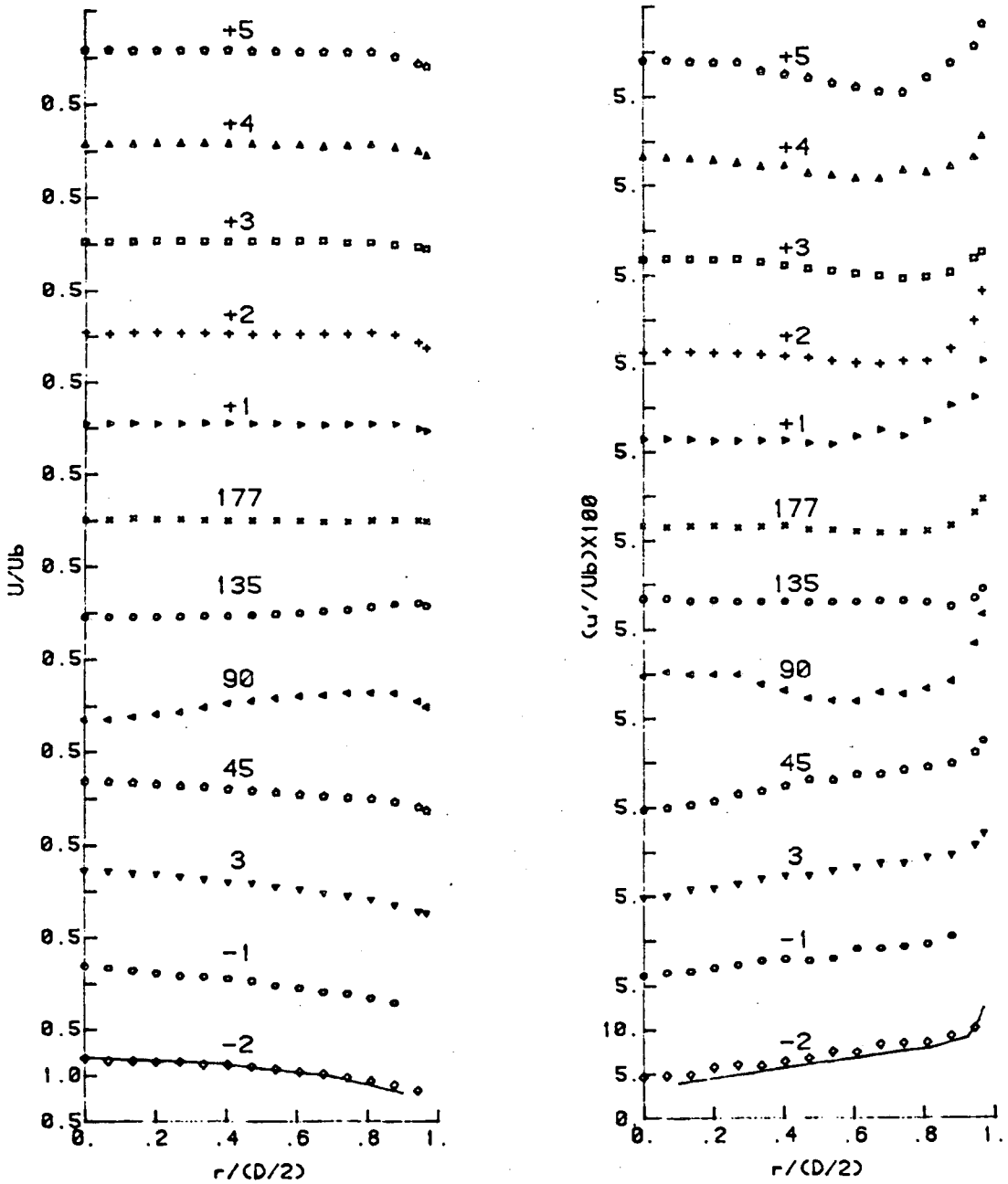

Figure 2. Longitudinal components of mean velocity and turbulence intensity in 180° curved pipe flow with Rc/D = 3.375, and Re = 57,400; (——) is Laufer's [19] data for Re = 50,000.

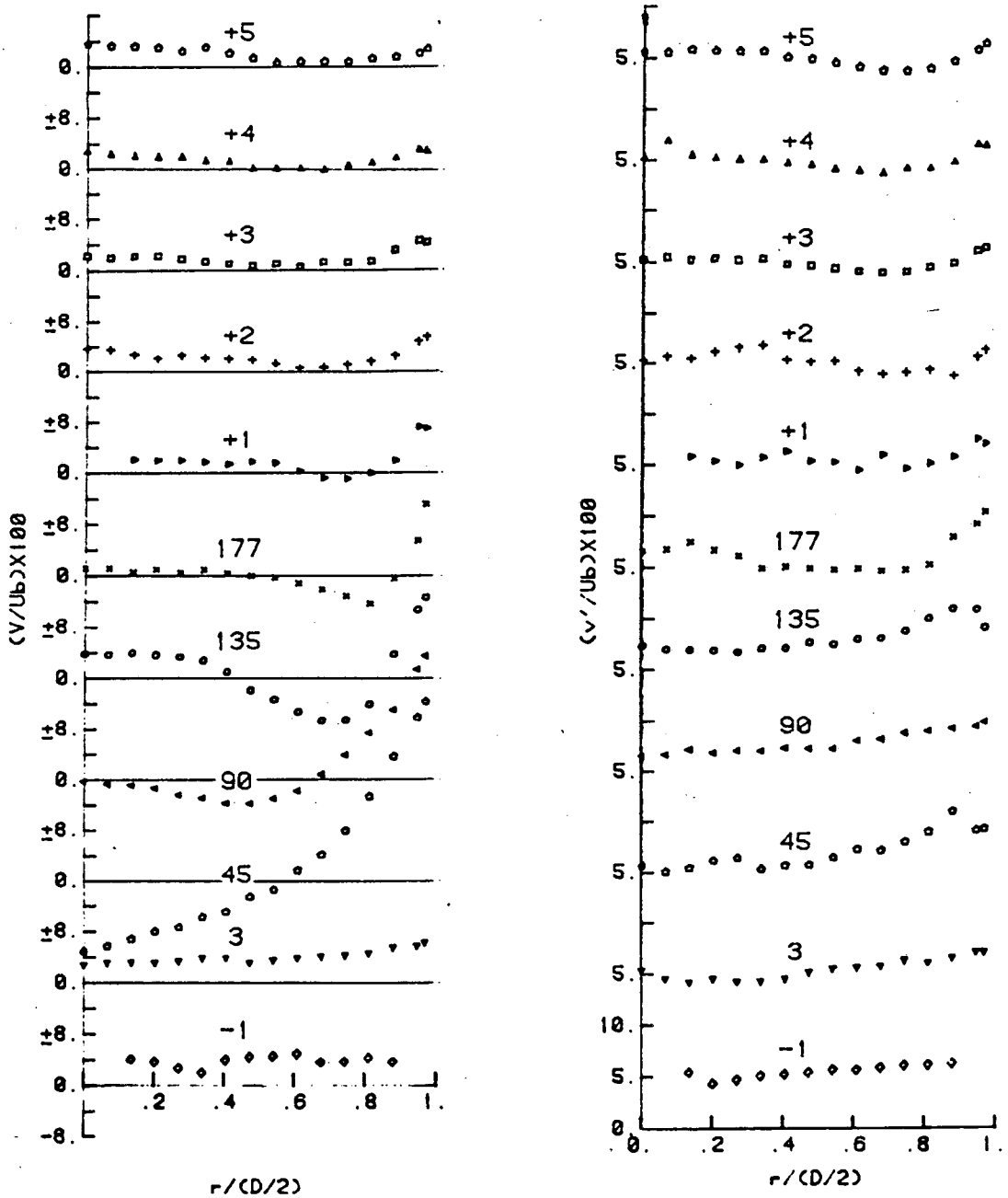

Figure 3. Circumferential components of mean velocity and turbulence intensity in 180° curved pipe flow with Rc/D = 3.375 and Re = 57,400.

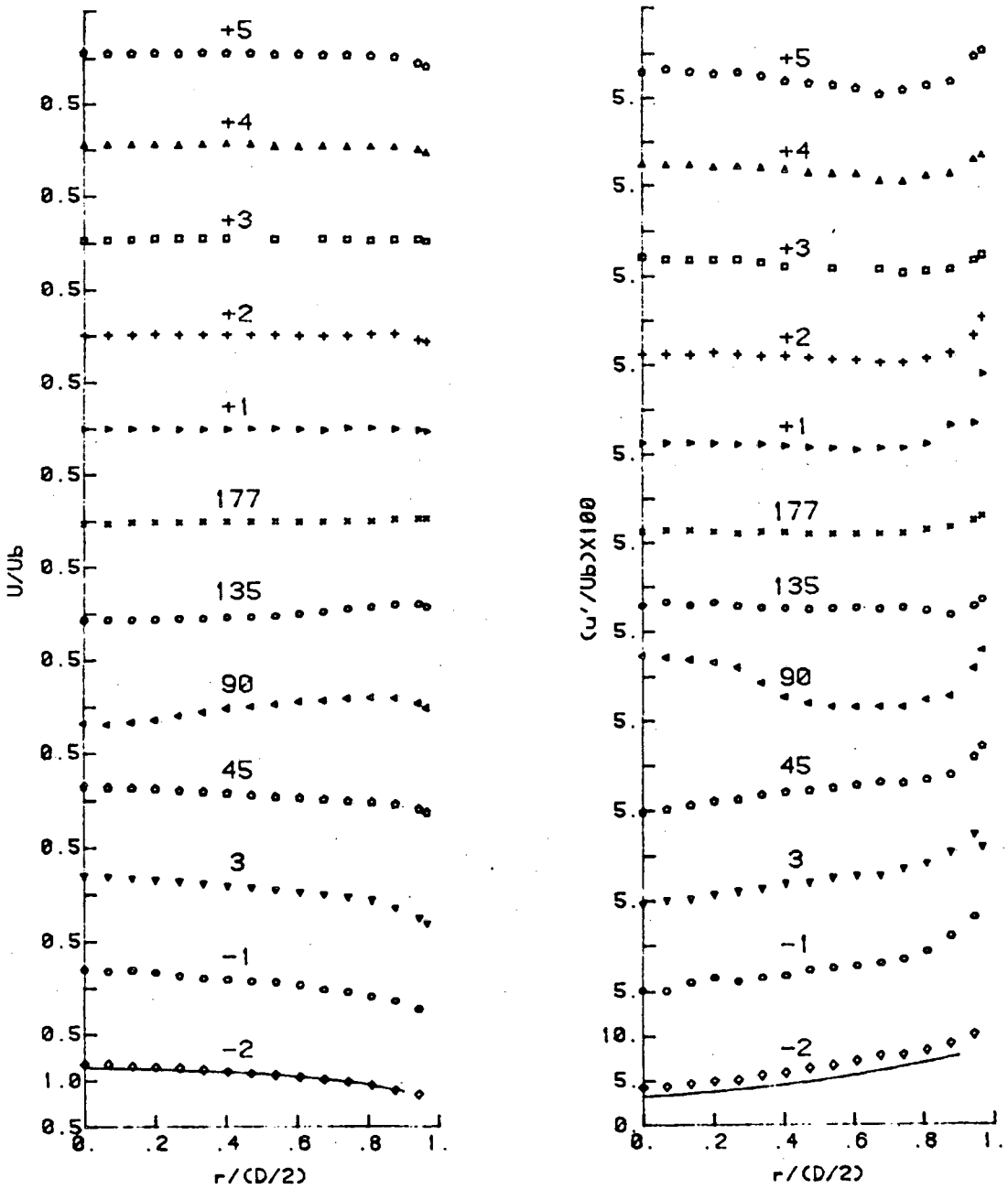

Figure 4. Longitudinal components of mean velocity and turbulence intensity in 180° curved pipe flow with Rc/D = 3.375 and Re = 110,000; (——) is Laufer's [19] data for Re = 500,000.

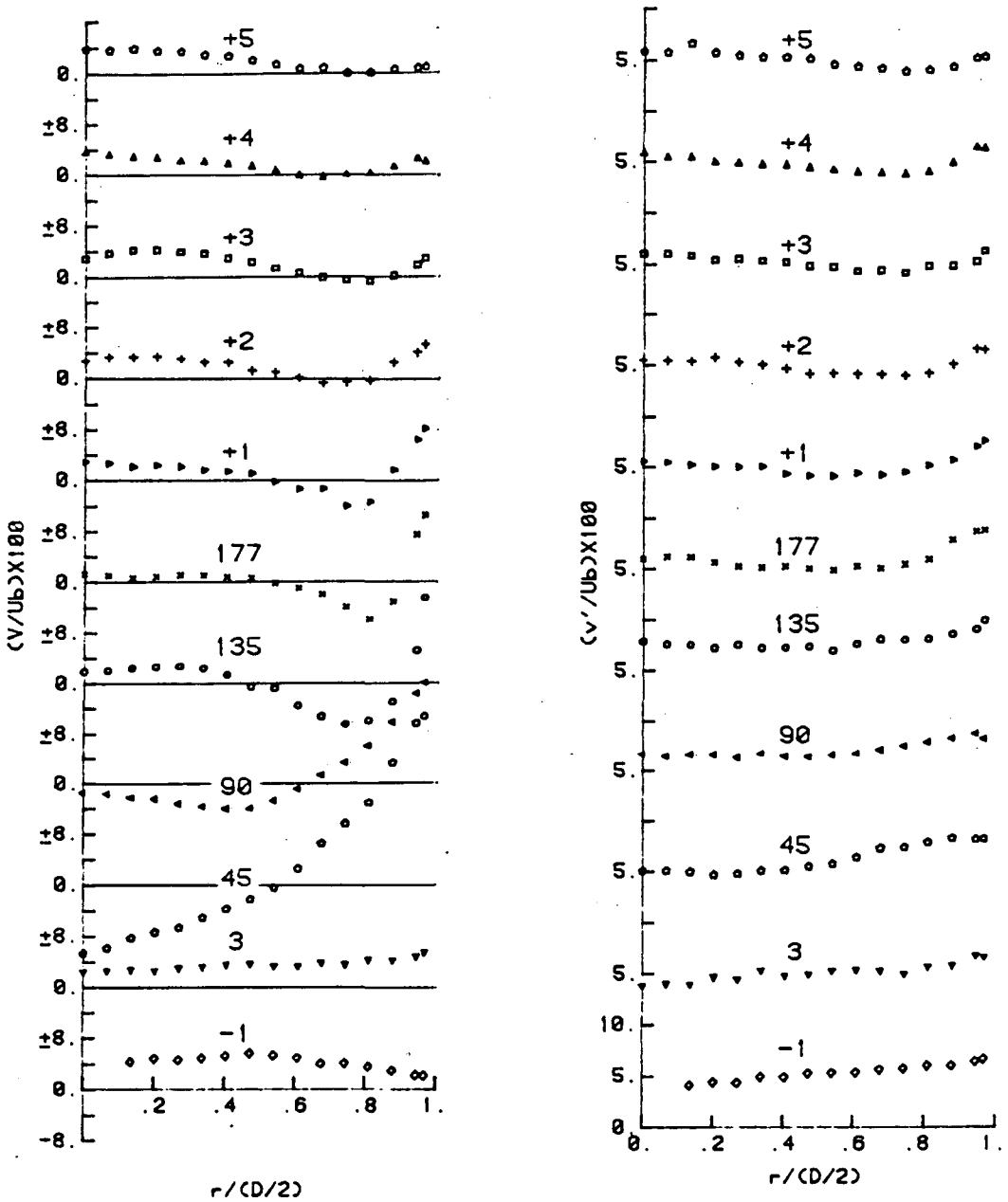

Figure 5. Circumferential components of mean velocity and turbulence intensity in 180° curved pipe flow with Rc/D = 3.375 and Re = 110,000.

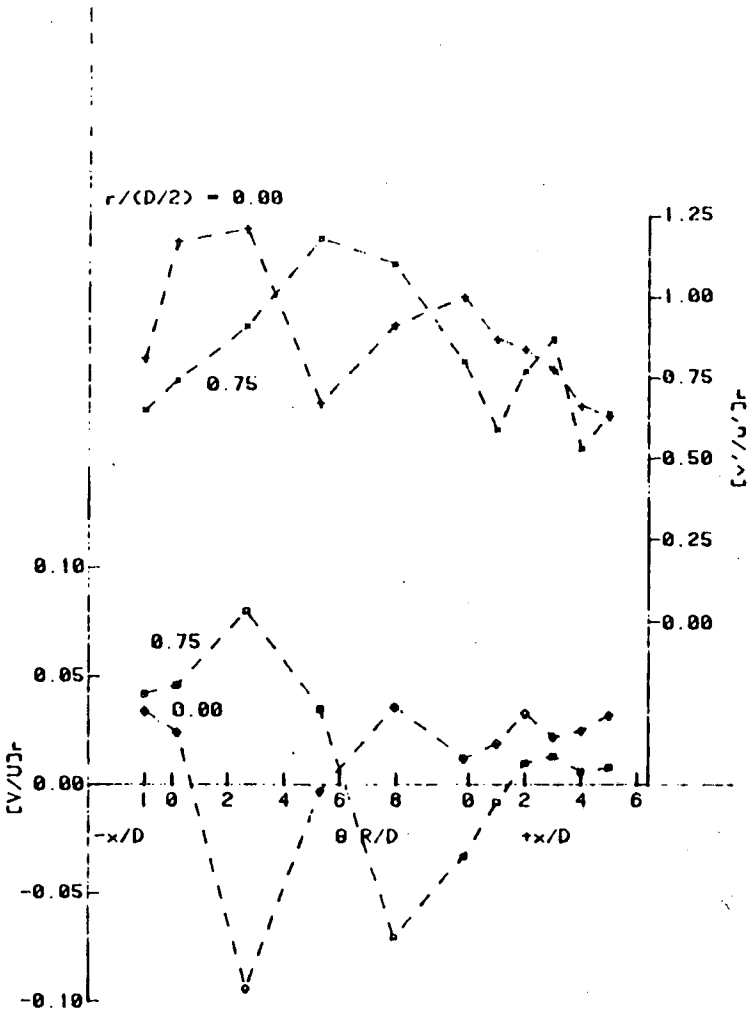

Figure 6. Ratios of circumferential-to-longitudinal mean velocities and turbulence intensities in 180° curved pipe flow with Rc/D = 3.375 and Re = 57,400.

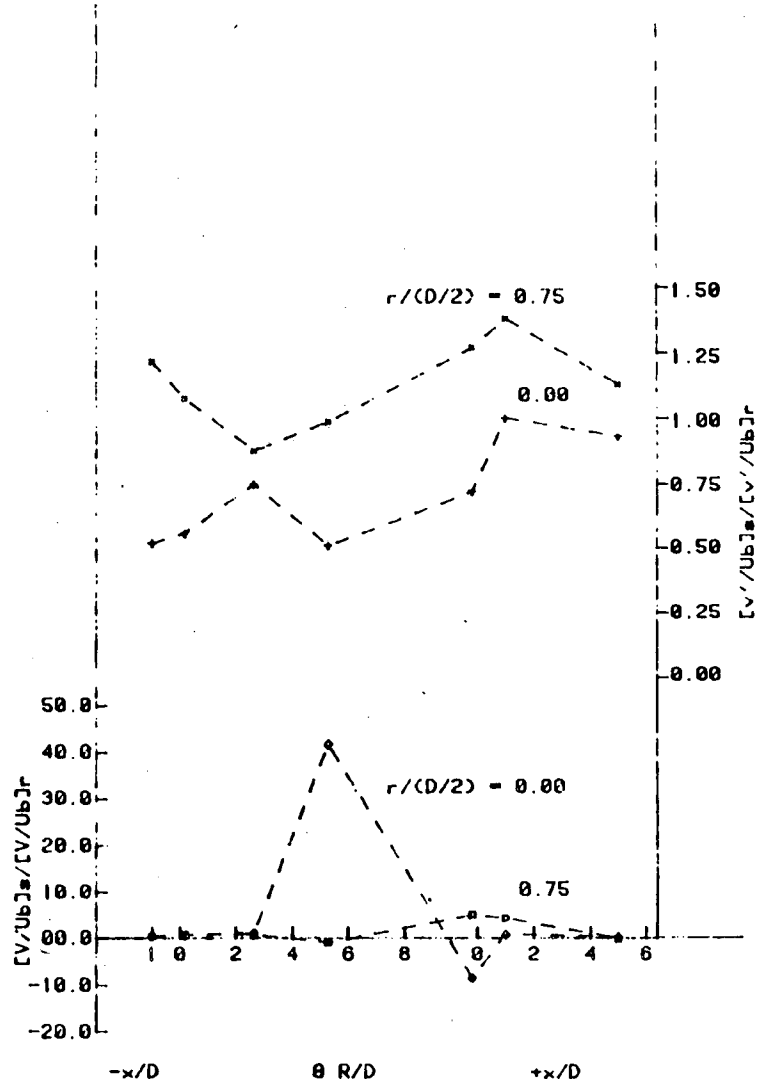

Figure 7. Ratios of the circumferential mean velocities and turbulence intensities in a 180° curved duct of square cross-section to corresponding values in a 180° curved pipe for similar Rc/D and Re.

APPENDIX I

Derivation of Beam Location and Velocity Correction Formulae

Nomenclature

d wall thickness

f_D Doppler frequency

r real beam intersection location in water (relative to pipe center)

r_v virtual beam intersection location in air (relative to pipe center)

R pipe inner radius

U "corrected" longitudinal (streamwise) velocity; obtained using $\psi = \gamma$ in $U = f_D \lambda/(2 \sin \psi)$

U_M measured longitudinal velocity; obtained by using $\psi = \alpha$ in $U_M = f_D \lambda/(2 \sin \psi)$

V "corrected" circumferential (cross-stream) velocity; obtained by using $\psi = \gamma$ in $V = f_D \lambda/(2 \sin \psi)$

V_M measured circumferential velocity; obtained by using $\psi = \alpha$ in $V_M = f_D \lambda/(2 \sin \psi)$

α half angle between light beams in air

γ half angle between light beams in water

n_f refractive index of water (relative to air)

n_p refractive index of plexiglass (relative to air)

λ wavelength of laser light

Longitudinal Velocity Component - Straight and Curved Pipe Sections

(See Figure I-1)

Assume small angles throughout such that:

sin (angle) ≈ tan (angle) ≈ angle

From Snell's law,

$$\sin \alpha = n_p \sin \beta \quad .$$

For small angles α, β ,

$$\beta \approx \alpha / n_p \quad . \tag{1}$$

From the geometry of Fig. I-1,

$$a = (R + d - r_v) \tan \alpha \approx (R + d - r_v)\, \alpha \quad ,$$

$$f = d \tan \beta \approx d\, \alpha / n_p \quad .$$

From Snell's law,

$$\sin \gamma = \frac{n_p}{n_f} \sin \beta \quad .$$

With (1) and a small angle approximation for γ,

$$\gamma \approx \alpha / n_f \quad . \tag{2}$$

Solving for r from geometry along with the above relations for a, f and γ:

$$R - r = (a - f)/\tan \gamma \approx \alpha\, [R - r_v + d\, (1 - 1/n_p)]\, n_f/\alpha$$

or,

$$R - r = [R - r_v + d\, (1 - 1/n_p)]\, n_f \quad ,$$

$$r = [R\, (1/n_f - 1) + r_v - d\, (1 - 1/n_p)]\, n_f \quad ,$$

$$\frac{r_v}{r} = \frac{1}{n_f} + \frac{R}{r}\, (1 - 1/n_f) + \frac{d}{r}\, (1 - 1/n_p) \quad . \tag{3}$$

Because

$$U_M \sim \frac{1}{\sin \alpha} \quad ,$$

it follows that

$$U = \sin \alpha \; U_M / \sin \gamma \simeq \alpha \; U_M / \gamma \quad .$$

Then from (2):

$$U = \eta_f \; U_M \tag{4}$$

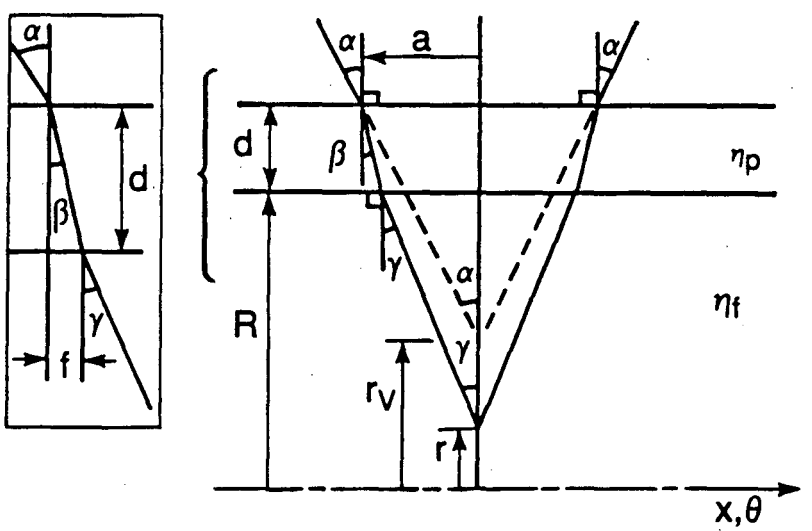

XBL 844-9341

Fig. I-1. Effect of parallel flat surfaces on beam intersection location and half angle; not to scale.

Circumferential Velocity Component - Straight Pipe Section (See Figure I-2)

From Snell's law and small angle approximations:

$$\delta_1 = \beta/n_p \quad , \tag{5}$$

$$\delta_2 = \sigma\ n_f/n_p \quad . \tag{6}$$

From the law of sines and small angle approximations:

$$\delta_2/\delta_1 = (R + d)/R \quad , \tag{7}$$

$$\gamma/\sigma = R/r \quad . \tag{8}$$

As approximations to a, with small angles:

$$a \simeq (R + d - r_v)\ \alpha$$

and

$$a \simeq (R + d)\ (\alpha - \beta) \quad .$$

Equating these expressions yields,

$$\beta = r_v\ \alpha/(R + d) \quad . \tag{9}$$

From (5), (6) and (7),

$$\sigma = (R + d)\ \beta/(R\ n_f) \quad . \tag{10}$$

From (9) and (10),

$$\sigma = r_v\ \alpha/(R\ n_f) \quad . \tag{11}$$

From (8) and (11),

$$r = \frac{r_v}{n_f} \frac{\alpha}{\gamma} \tag{12}$$

We now seek an expression for γ/α, the half angle correction factor. From geometrical considerations, we may use the following approximations for e:

$$\frac{e}{\alpha - \beta - \gamma + \sigma} \approx \frac{R}{\sin 90^\circ} = R \quad ,$$

$$e \approx d\,\delta_1$$

Then, from the above two expressions,

$$\alpha - \beta - \gamma + \sigma = \frac{d}{R}\delta_1 \quad .$$

Introducing (5), (9) and (11),

$$\alpha - \frac{r_v\ \alpha}{R + d} - \gamma + \frac{r_v\,\alpha}{R\,n_f} = \frac{d}{R}\frac{\beta}{n_p} = \frac{d}{R}\frac{r_v\,\alpha}{(R + d)\,n_p} \quad .$$

Dividing by α,

$$1 - \frac{r_v}{R + d} - \gamma/\alpha + \frac{r_v}{R\,n_f} = \frac{d}{R}\frac{r_v}{(R + d)\,n_p} \quad .$$

Solving for γ/α:

$$\frac{\gamma}{\alpha} = 1 - \frac{d}{R}\frac{r_v}{(R + d)\,n_p} - \frac{r_v}{(R + d)} + \frac{r_v}{R\,n_f}$$

or, equivalently,

$$\frac{\gamma}{\alpha} = \frac{r_v}{R + d}\left[\frac{R + d}{R\,n_f} - 1 - \frac{d}{R\,n_p}\right] + 1 \quad ,$$

(12) then becomes

$$\frac{r_v}{r} = \eta_f/[1 - \frac{r\,\eta_f}{R + d}\,(\frac{R + d}{R\,\eta_f} - 1 - \frac{d}{R\,\eta_p})] \tag{13}$$

Because

$$V = V_M \sin\alpha/\sin\gamma \approx \alpha\, V_M/\gamma \quad ,$$

we may solve for V,

$$V = \frac{V_M}{1 + \frac{r_v}{R + d}\,[\frac{R + d}{R\,\eta_f} - 1 - \frac{d}{R\,\eta_p}]} \tag{14}$$

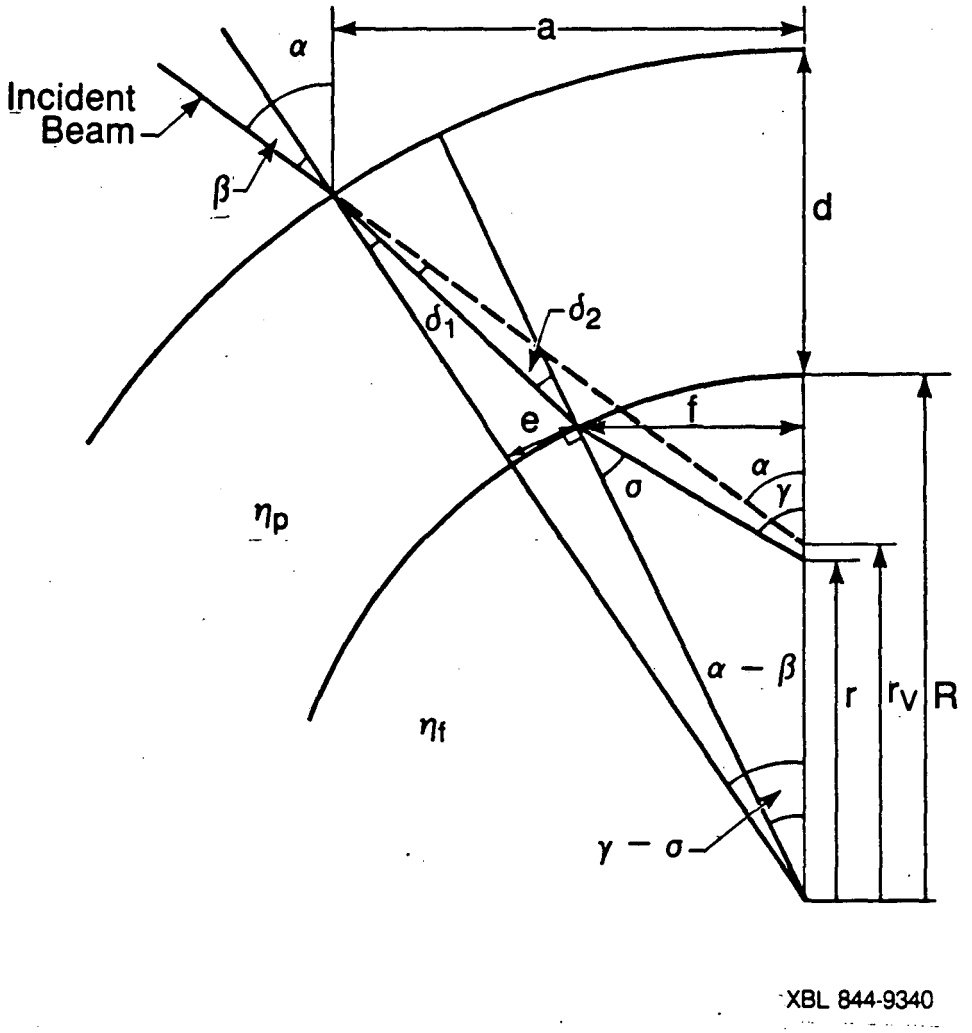

Fig. I-2 Effect of concentric curved surfaces on beam intersection location and half angle; not to scale.

Circumferential Velocity Component - Curved Pipe Section (See Figure I-3)

Snell's law and small angle approximations yield:

$$\beta \simeq \alpha/\eta_p \quad , \tag{15}$$

$$\psi \simeq \omega\, \eta_p/\eta_f \quad . \tag{16}$$

From the geometry of Fig. I-3 and using (15),

$$a = (R + d - r_v)\, \alpha \quad ,$$

$$\omega = \beta - \sigma \quad ,$$

$$f = b \tan \beta \simeq d \tan \beta \simeq d\, \beta = d \frac{\alpha}{\eta_p}$$

$$g = a - f = [R + d\, (1 - 1/\eta_p) - r_v]\, \alpha \quad ,$$

and with the preceding expression for g,

$$\sigma = \sin^{-1} g/R \simeq \alpha\, [1 - r_v/R + d/R\, (1 - 1/\eta_p)] \quad . \tag{17}$$

From (15) and (17) substituted into the expression for ω,

$$\omega = \alpha\, [1/\eta_p - 1 + r_v/R - d/R\, (1 - 1/\eta_p)]$$

or

$$\omega = \alpha\, [r_v/R - (1 + d/R)\, (1 - 1/\eta_p)] \quad . \tag{18}$$

Using (16) and (18),

$$\psi = \alpha\, [(\frac{r_v}{R})\, \frac{\eta_p}{\eta_f} - (1 + d/R)\, (\frac{\eta_p}{\eta_f} - \frac{1}{\eta_f})] \quad . \tag{19}$$

From the geometry of Fig. I-3,

$$h = r \sin\sigma = (R - r\cos\sigma)\tan\psi \quad .$$

Solving for r with small angles σ, ψ:

$$r \simeq R\,\psi/(\psi + \sigma) \quad .$$

This becomes, with (17) and (19):

$$r = \frac{R\left[\frac{r_v}{R}\frac{n_p}{n_f} - (1 + d/R)\left(\frac{n_p}{n_f} - 1/n_f\right)\right]}{1 + \frac{r_v}{R}\left(\frac{n_p}{n_f} - 1\right) + \frac{d}{R}\left(1 - 1/n_p + 1/n_f - \frac{n_p}{n_f}\right) + 1/n_f - \frac{n_p}{n_f}}$$

or

$$\frac{r_v}{r} = R\left[\frac{R}{r}(1 + d/R)(n_p/n_f - 1/n_f)\right.$$

$$\left. + 1 + d/R\,(1 - 1/n_p + 1/n_f - n_p/n_f) + 1/n_f - n_p/n_f\right] \tag{20}$$

$$/\left[(1 - n_p/n_f)\,r + R\,n_p/n_f\right]$$

Here γ is defined by

$$\gamma = \sigma + \psi$$

and can be found using (17) and (19).

Since the expression for V is given by

$$V = V_M \frac{\sin\alpha}{\sin\gamma} \simeq V_M \frac{\alpha}{\gamma} = V_M \frac{\alpha}{\sigma + \psi} \quad ,$$

it follows that,

$$V = \frac{V_M}{1 - \frac{n_p - 1}{n_f} + \frac{r_v}{R}\left(\frac{n_p}{n_f} - 1\right) + \frac{d}{R}\left(\frac{n_p - 1}{n_p} - \frac{n_p - 1}{n_f}\right)} \quad . \tag{21}$$

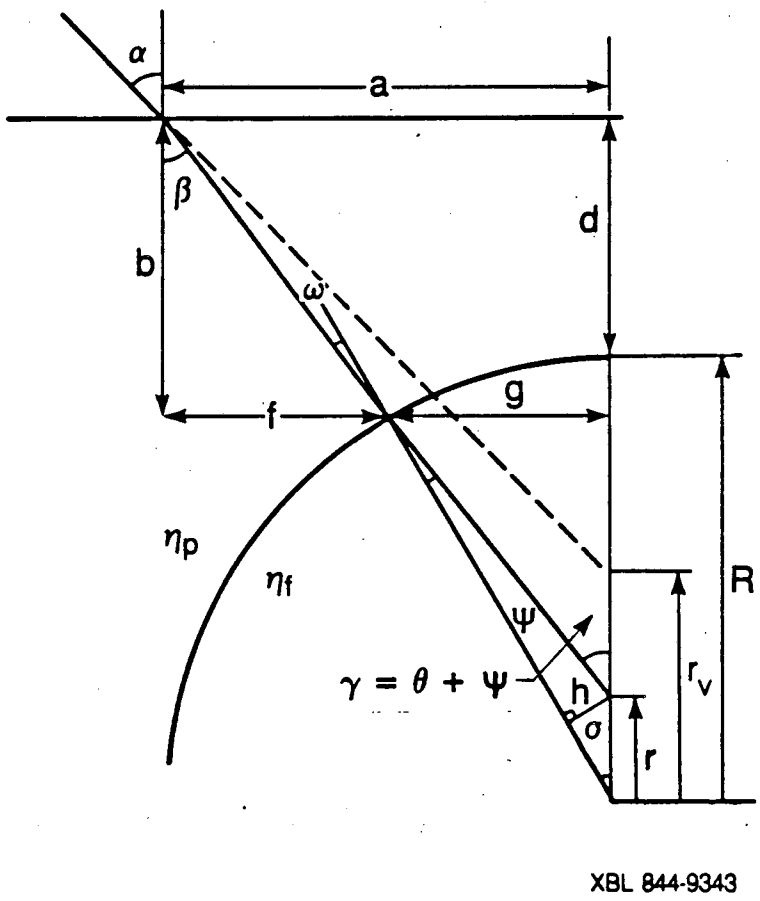

Fig. I-3. Effect of flat-to-curved surfaces on beam intersection location and half angle; not to scale.

APPENDIX II

Frequency Shifting Procedure

The electronic downmixer is one of two modular units on the DISA 55 N11-16 frequency shifting device. Either one of two channels (A or B) may be used. The photomultiplier (PM) output signal cable is attached to the PM IN port in the rear of the downmixer and another is attached from the MIXER OUT to the PM SIGNAL IN port of the DISA counter. The least complicated mode of operation is to set the net electronic shift, f_s, greater than the maximum frequency expected in the flow. For instance, if a maximum center line velocity of 5 m/s is expected, with an estimated minimum calibration fringe factor based on the optical parameters and test section geometry of 10 m/s/MHz, then a simple ratio gives a 0.5 MHz upper frequency estimate.

With the shift frequency denoted by f_{Lo} and signal frequency by f_o, we would then set the shift dial corresponding to $f_{Lo} < 40$ MHz to a value slightly greater than 0.5 MHz, say 700 KHz. The signal from the counter, monitored on the oscilloscope, now has a net positive mixer frequency shift imposed. In the computer program for evaluating velocity, the shift value f_{Lo} must be subtracted from the frequency measured by the counter. In the present example, we would add -0.7 MHz to each measured Doppler count. Values of velocity computed in this manner are either positive or negative, depending on the direction in which the fringes are moving. The fringe movement is set by turning the Bragg cell screw.

A verification of fringe sense of translation is necessary. A rotating diffraction grating, with the laser beams intersecting just on the grating surface, can be used to achieve this. Computed values of velocity and their

signs for prescribed speeds and sense of grating rotation should agree with the physically (known) imposed conditions. Wherever the calculated sign of velocity is positive the fringes are moving opposite to the grating direction; the opposite is true for negative values of velocity.

If a mirror is used to divert the beam path, as in the present case, care must be taken to note which way the fringes move after beam reflection.

APPENDIX III

DATA TABULATION

The following is a listing of measurements obtained at various longitudinal stations in the test section. Scans were always performed along the radial direction, in the plane $\phi = \pi/2$ (see Fig. 1). Both unweighted and weighted results are tabulated. For weighting the one-dimensional scheme proposed by McLaughlin and Tiederman [17] was used. Differences between weighted and unweighted data are discussed in the text where it is concluded that weighting the circumferential components, V and v', yields unrealistic results.

x/D = -2

Weighted Data

	Re = 57,400				Re = 110,000			
r/(D/2)	U/Ub	u'/Ub	V/Ub	v'/Ub	U/Ub	u'/Ub	V/Ub	v'/Ub
0.967	----	-----			----	-----		
0.945	0.84	0.102			0.85	0.101		
0.877	0.90	0.093	<.005	<.040	0.90	0.091	<.005	<.040
0.810	0.94	0.086			0.95	0.086		
0.742	0.98	0.085			0.99	0.085		
0.675	1.02	0.084			1.01	0.084		
0.607	1.04	0.075			1.04	0.075		
0.540	1.07	0.076			1.06	0.076		
0.472	1.10	0.068			1.08	0.068		
0.405	1.12	0.065			1.10	0.059		
0.337	1.12	0.060			1.12	0.056		
0.270	1.12	0.061			1.14	0.051		
0.202	1.15	0.058			1.15	0.050		
0.135	1.16	0.050			1.16	0.047		
0.067	1.16	0.048			1.18	0.043		
0.000	1.19	0.047			1.18	0.043		

Unweighted Data

	Re = 57,400				Re = 110,000			
r/(D/2)	U/Ub	u'/Ub	V/Ub	v'/Ub	U/Ub	u'/Ub	V/Ub	v'/Ub
0.967	----	-----			----	-----		
0.945	0.85	0.102			0.86	0.098		
0.877	0.91	0.087	<.015	<.075	0.91	0.092	<.015	<.075
0.810	0.95	0.085			0.96	0.083		
0.742	0.98	0.084			1.00	0.079		
0.675	1.03	0.083			1.02	0.077		
0.607	1.05	0.075			1.05	0.071		
0.540	1.08	0.075			1.07	0.066		
0.472	1.11	0.067			1.09	0.063		
0.405	1.12	0.065			1.11	0.059		
0.337	1.13	0.060			1.12	0.055		
0.270	1.15	0.061			1.14	0.051		
0.202	1.16	0.057			1.15	0.049		
0.135	1.16	0.049			1.16	0.047		
0.067	1.16	0.048			1.18	0.043		
0.000	1.19	0.046			1.18	0.043		

x/D = -1

Weighted Data

	Re = 57,400				Re = 110,000			
r/(D/2)	U/Ub	u'/Ub	V/Ub	v'/Ub	U/Ub	u'/Ub	V/Ub	v'/Ub
0.967	----	-----	-----	-----	----	-----	0.006	0.034
0.945	----	-----	-----	-----	0.77	0.133	0.006	0.032
0.877	0.79	0.107	0.012	0.037	0.85	0.113	0.008	0.031
0.810	0.84	0.102	0.015	0.038	0.90	0.094	0.010	0.033
0.742	0.89	0.097	0.014	0.037	0.95	0.088	0.012	0.033
0.675	0.89	0.091	0.013	0.034	0.98	0.082	0.013	0.033
0.607	0.93	0.085	0.019	0.038	1.03	0.084	0.016	0.035
0.540	0.95	0.083	0.016	0.036	1.06	0.076	0.019	0.035
0.472	1.03	0.083	0.016	0.035	1.07	0.073	0.020	0.036
0.405	1.05	0.084	0.015	0.032	1.08	0.067	0.018	0.033
0.337	1.07	0.084	0.007	0.029	1.10	0.065	0.016	0.032
0.270	1.08	0.076	0.010	0.028	1.13	0.064	0.017	0.030
0.202	1.11	0.072	0.015	0.029	1.16	0.067	0.018	0.031
0.135	1.12	0.071	0.018	0.032	1.18	0.060	0.016	0.028
0.067	1.16	0.070	-----	-----	1.18	0.051	-----	-----
0.000	1.17	0.064	-----	-----	1.19	0.051	-----	-----

Unweighted Data

	Re = 57,400				Re = 110,000			
r/(D/2)	U/Ub	u'/Ub	V/Ub	v'/Ub	U/Ub	u'/Ub	V/Ub	v'/Ub
0.967	----	-----	-----	-----	----	-----	0.022	0.067
0.945	----	-----	-----	-----	0.77	0.132	0.023	0.065
0.877	0.81	0.103	0.037	0.063	0.86	0.111	0.030	0.060
0.810	0.85	0.101	0.043	0.062	0.90	0.094	0.036	0.060
0.742	0.90	0.096	0.038	0.062	0.95	0.085	0.041	0.058
0.675	0.91	0.091	0.037	0.059	0.98	0.081	0.040	0.054
0.607	0.94	0.085	0.050	0.057	1.03	0.078	0.049	0.053
0.540	0.96	0.083	0.046	0.057	1.06	0.077	0.053	0.053
0.472	1.03	0.083	0.045	0.055	1.07	0.073	0.057	0.053
0.405	1.05	0.083	0.040	0.053	1.09	0.067	0.053	0.049
0.337	1.09	0.082	0.021	0.051	1.10	0.065	0.049	0.049
0.270	1.09	0.075	0.028	0.047	1.13	0.061	0.046	0.044
0.202	1.12	0.071	0.037	0.043	1.17	0.065	0.049	0.044
0.135	1.13	0.070	0.041	0.054	1.19	0.060	0.043	0.041
0.067	1.16	0.068	-----	-----	1.18	0.051	-----	-----
0.000	1.17	0.062	-----	-----	1.20	0.051	-----	-----

$\theta = 3^\circ$

Weighted Data

	Re = 57,400				Re = 110,000			
r/(D/2)	U/Ub	u'/Ub	V/Ub	v'/Ub	U/Ub	u'/Ub	V/Ub	v'/Ub
0.967	0.76	0.122	0.024	0.047	0.69	0.111	0.017	0.040
0.945	0.78	0.107	0.022	0.046	0.75	0.124	0.015	0.040
0.877	0.85	0.099	0.020	0.044	0.86	0.104	0.013	0.035
0.810	0.91	0.095	0.018	0.041	0.94	0.092	0.013	0.033
0.742	0.95	0.088	0.016	0.039	0.97	0.086	0.012	0.029
0.675	0.98	0.087	0.016	0.037	1.00	0.078	0.012	0.031
0.607	1.02	0.084	0.015	0.036	1.02	0.078	0.011	0.029
0.540	1.05	0.080	0.014	0.034	1.05	0.076	0.012	0.030
0.472	1.09	0.080	0.015	0.032	1.07	0.071	0.013	0.030
0.405	1.10	0.074	0.016	0.031	1.09	0.070	0.014	0.028
0.337	1.13	0.071	0.017	0.030	1.12	0.064	0.012	0.028
0.270	1.16	0.065	0.015	0.029	1.14	0.061	0.012	0.028
0.202	1.19	0.060	0.015	0.028	1.16	0.058	0.010	0.025
0.135	1.20	0.059	0.015	0.028	1.17	0.053	0.011	0.024
0.067	1.22	0.051	0.016	0.028	1.19	0.051	0.011	0.024
0.000	1.23	0.049	0.014	0.029	1.20	0.047	0.010	0.023

Unweighted Data

	Re = 57,400				Re = 110,000			
r/(D/2)	U/Ub	u'/Ub	V/Ub	v'/Ub	U/Ub	u'/Ub	V/Ub	v'/Ub
0.967	0.78	0.143	0.066	0.074	0.71	0.114	0.057	0.067
0.945	0.80	0.109	0.059	0.074	0.75	0.124	0.050	0.069
0.877	0.86	0.099	0.056	0.069	0.86	0.104	0.044	0.060
0.810	0.91	0.094	0.048	0.063	0.94	0.091	0.046	0.058
0.742	0.95	0.088	0.044	0.065	0.97	0.086	0.037	0.051
0.675	0.98	0.088	0.043	0.059	1.00	0.078	0.039	0.054
0.607	1.02	0.083	0.041	0.057	1.02	0.077	0.034	0.055
0.540	1.06	0.079	0.037	0.057	1.05	0.075	0.035	0.054
0.472	1.09	0.073	0.033	0.053	1.07	0.070	0.038	0.051
0.405	1.11	0.074	0.040	0.046	1.09	0.070	0.037	0.049
0.337	1.14	0.070	0.040	0.044	1.12	0.064	0.034	0.054
0.270	1.17	0.064	0.035	0.043	1.14	0.060	0.031	0.045
0.202	1.19	0.058	0.032	0.046	1.16	0.057	0.027	0.048
0.135	1.21	0.057	0.033	0.043	1.17	0.052	0.029	0.041
0.067	1.22	0.050	0.033	0.046	1.19	0.050	0.027	0.041
0.000	1.23	0.046	0.029	0.054	1.20	0.046	0.026	0.039

$\theta = 45^{0}$

Weighted Data

	Re = 57,400				Re = 110,000			
r/(D/2)	U/Ub	u'/Ub	V/Ub	v'/Ub	U/Ub	u'/Ub	V/Ub	v'/Ub
0.967	0.85	0.125	0.224	0.119	0.85	0.122	0.226	0.098
0.945	0.89	0.111	0.193	0.118	0.89	0.109	0.204	0.107
0.877	0.95	0.099	0.119	0.105	0.94	0.089	0.125	0.095
0.810	0.98	0.095	0.065	0.074	0.96	0.084	0.055	0.068
0.742	0.99	0.092	0.029	0.054	0.97	0.080	0.032	0.055
0.675	1.01	0.087	0.013	0.041	0.99	0.081	0.017	0.041
0.607	1.03	0.087	0.005	0.038	1.01	0.078	0.007	0.032
0.540	1.05	0.081	-0.005	0.036	1.02	0.075	-0.002	0.029
0.472	1.07	0.081	-0.009	0.034	1.04	0.072	-0.007	0.030
0.405	1.09	0.074	-0.018	0.038	1.06	0.070	-0.011	0.031
0.337	1.11	0.068	-0.023	0.040	1.08	0.067	-0.016	0.034
0.270	1.12	0.065	-0.031	0.046	1.09	0.062	-0.027	0.039
0.202	1.14	0.057	-0.037	0.047	1.11	0.060	-0.032	0.042
0.135	1.16	0.053	-0.046	0.051	1.12	0.056	-0.039	0.046
0.067	1.17	0.049	-0.061	0.054	1.13	0.051	-0.053	0.052
0.000	1.18	0.047	-0.068	0.058	1.14	0.048	-0.061	0.054

Unweighted Data

	Re = 57,400				Re = 110,000			
r/(D/2)	U/Ub	u'/Ub	V/Ub	v'/Ub	U/Ub	u'/Ub	V/Ub	v'/Ub
0.967	0.87	0.121	0.286	0.096	0.87	0.119	0.268	0.083
0.945	0.91	0.107	0.261	0.094	0.90	0.103	0.257	0.083
0.877	0.95	0.095	0.199	0.113	0.95	0.087	0.193	0.084
0.810	0.98	0.093	0.135	0.093	0.96	0.083	0.130	0.080
0.742	1.00	0.091	0.080	0.083	0.98	0.078	0.096	0.075
0.675	1.01	0.085	0.041	0.074	1.00	0.078	0.065	0.074
0.607	1.04	0.086	0.017	0.075	1.02	0.077	0.025	0.064
0.540	1.05	0.081	-0.014	0.066	1.02	0.074	-0.005	0.058
0.472	1.08	0.080	-0.025	0.058	1.04	0.071	-0.022	0.056
0.405	1.10	0.072	-0.049	0.058	1.06	0.069	-0.037	0.052
0.337	1.12	0.067	-0.057	0.054	1.08	0.066	-0.051	0.052
0.270	1.13	0.064	-0.074	0.065	1.09	0.061	-0.066	0.049
0.202	1.15	0.057	-0.081	0.062	1.11	0.059	-0.074	0.048
0.135	1.16	0.051	-0.093	0.055	1.12	0.055	-0.083	0.051
0.067	1.17	0.048	-0.103	0.052	1.13	0.051	-0.098	0.051
0.000	1.19	0.047	-0.112	0.057	1.14	0.047	-0.106	0.051

$\theta = 90^\circ$

Weighted Data

	Re = 57,400				Re = 110,000			
r/(D/2)	U/Ub	u'/Ub	V/Ub	v'/Ub	U/Ub	u'/Ub	V/Ub	v'/Ub
0.967	0.98	0.167	0.099	0.104	0.98	0.129	0.083	0.086
0.945	1.04	0.133	0.086	0.094	1.03	0.109	0.065	0.079
0.877	1.13	0.092	0.043	0.069	1.09	0.078	0.031	0.057
0.810	1.13	0.084	0.022	0.055	1.09	0.074	0.016	0.043
0.742	1.13	0.078	0.011	0.046	1.08	0.066	0.008	0.036
0.675	1.11	0.080	0.002	0.042	1.06	0.066	-0.003	0.033
0.607	1.10	0.070	-0.005	0.041	1.05	0.066	-0.003	0.032
0.540	1.08	0.071	-0.009	0.040	1.02	0.066	-0.008	0.034
0.472	1.05	0.073	-0.009	0.039	1.00	0.070	-0.011	0.034
0.405	1.02	0.082	-0.010	0.040	0.98	0.077	-0.011	0.033
0.337	0.98	0.089	-0.007	0.037	0.94	0.093	-0.009	0.033
0.270	0.93	0.100	-0.005	0.037	0.90	0.110	-0.008	0.032
0.202	0.91	0.100	-0.002	0.036	0.86	0.116	-0.005	0.031
0.135	0.88	0.100	-0.000	0.036	0.83	0.119	-0.004	0.032
0.067	0.85	0.102	0.001	0.035	0.81	0.121	-0.003	0.031
0.000	0.85	0.098	0.002	0.034	0.82	0.123	-0.002	0.031

Unweighted Data

	Re = 57,400				Re = 110,000			
r/(D/2)	U/Ub	u'/Ub	V/Ub	v'/Ub	U/Ub	u'/Ub	V/Ub	v'/Ub
0.967	1.02	0.159	0.197	0.101	1.00	0.119	0.163	0.083
0.945	1.05	0.125	0.176	0.096	1.04	0.103	0.146	0.088
0.877	1.14	0.089	0.113	0.094	1.09	0.076	0.100	0.083
0.810	1.14	0.082	0.077	0.092	1.09	0.072	0.062	0.079
0.742	1.14	0.076	0.040	0.090	1.08	0.065	0.035	0.071
0.675	1.12	0.073	0.010	0.083	1.06	0.066	0.014	0.068
0.607	1.10	0.069	-0.017	0.082	1.05	0.066	-0.008	0.066
0.540	1.08	0.070	-0.029	0.073	1.03	0.066	-0.027	0.065
0.472	1.05	0.072	-0.036	0.074	1.01	0.070	-0.039	0.065
0.405	1.02	0.081	-0.036	0.074	0.98	0.076	-0.040	0.068
0.337	0.98	0.087	-0.028	0.071	0.95	0.089	-0.036	0.064
0.270	0.95	0.098	-0.024	0.072	0.91	0.104	-0.032	0.067
0.202	0.91	0.098	-0.013	0.069	0.87	0.112	-0.025	0.064
0.135	0.88	0.098	-0.008	0.073	0.85	0.118	-0.023	0.067
0.067	0.87	0.102	-0.007	0.067	0.83	0.121	-0.017	0.064
0.000	0.87	0.098	-0.003	0.066	0.84	0.121	-0.015	0.066

$\theta = 135°$

Weighted Data

	Re = 57,400				Re = 110,000			
r/(D/2)	U/Ub	u'/Ub	V/Ub	v'/Ub	U/Ub	u'/Ub	V/Ub	v'/Ub
0.967	1.06	0.095	0.052	0.074	1.06	0.086	0.044	0.074
0.945	1.09	0.084	0.040	0.074	1.09	0.078	0.013	0.046
0.877	1.08	0.075	0.011	0.056	1.09	0.068	-0.006	0.041
0.810	1.05	0.080	-0.012	0.054	1.06	0.073	-0.017	0.047
0.742	1.02	0.082	-0.022	0.056	1.04	0.077	-0.018	0.047
0.675	1.01	0.082	-0.023	0.053	1.01	0.075	-0.014	0.043
0.607	0.99	0.081	-0.015	0.048	0.99	0.077	-0.008	0.038
0.540	0.98	0.081	-0.009	0.042	0.97	0.076	-0.008	0.033
0.472	0.97	0.080	-0.005	0.041	0.96	0.075	0.000	0.035
0.405	0.96	0.081	0.004	0.039	0.95	0.076	0.005	0.035
0.337	0.96	0.081	0.012	0.041	0.94	0.077	0.008	0.038
0.270	0.95	0.081	0.013	0.041	0.94	0.079	0.010	0.039
0.202	0.95	0.083	0.015	0.042	0.93	0.083	0.008	0.040
0.135	0.95	0.082	0.017	0.044	0.93	0.080	0.008	0.039
0.067	0.95	0.084	0.014	0.044	0.93	0.083	0.007	0.039
0.000	0.95	0.084	0.017	0.046	0.93	0.079	0.006	0.041

Unweighted Data

	Re = 57,400				Re = 110,000			
r/(D/2)	U/Ub	u'/Ub	V/Ub	v'/Ub	U/Ub	u'/Ub	V/Ub	v'/Ub
0.967	1.07	0.092	0.127	0.092	1.07	0.084	0.135	0.098
0.945	1.09	0.082	0.108	0.110	1.09	0.077	0.052	0.089
0.877	1.09	0.074	0.037	0.110	1.09	0.068	-0.030	0.085
0.810	1.06	0.079	-0.041	0.101	1.06	0.072	-0.059	0.080
0.742	1.03	0.081	-0.067	0.089	1.04	0.076	-0.065	0.079
0.675	1.02	0.081	-0.068	0.082	1.02	0.074	-0.053	0.080
0.607	0.98	0.081	-0.053	0.080	0.99	0.076	-0.036	0.076
0.540	0.98	0.079	-0.034	0.076	0.98	0.075	-0.009	0.069
0.472	0.97	0.084	-0.019	0.072	0.97	0.075	-0.006	0.073
0.405	0.96	0.081	0.009	0.071	0.96	0.075	0.013	0.072
0.337	0.96	0.081	0.027	0.071	0.95	0.077	0.023	0.072
0.270	0.96	0.081	0.032	0.068	0.94	0.078	0.027	0.075
0.202	0.95	0.083	0.035	0.069	0.94	0.082	0.026	0.072
0.135	0.98	0.082	0.038	0.070	0.93	0.080	0.023	0.075
0.067	0.96	0.084	0.036	0.070	0.94	0.083	0.020	0.075
0.000	0.95	0.081	0.037	0.074	0.94	0.079	0.018	0.078

$\theta = 177^\circ$

Weighted Data

	Re = 57,400				Re = 110,000			
r/(D/2)	U/Ub	u'/Ub	V/Ub	v'/Ub	U/Ub	u'/Ub	V/Ub	v'/Ub
0.967	0.98	0.096	0.042	0.067	1.02	0.081	0.032	0.060
0.945	0.99	0.081	0.015	0.053	1.02	0.076	0.020	0.049
0.877	1.00	0.067	-0.002	0.042	1.02	0.068	-0.008	0.040
0.810	0.99	0.061	-0.016	0.034	1.00	0.065	-0.016	0.037
0.742	0.98	0.059	-0.011	0.030	1.00	0.061	-0.010	0.029
0.675	0.98	0.059	-0.007	0.028	0.99	0.060	-0.004	0.025
0.607	0.99	0.060	-0.004	0.028	0.99	0.060	-0.001	0.025
0.540	1.00	0.062	0.001	0.028	1.00	0.060	0.002	0.024
0.472	1.00	0.062	0.002	0.027	1.00	0.060	0.004	0.025
0.405	1.00	0.067	0.003	0.029	1.00	0.062	0.004	0.026
0.337	1.00	0.066	0.005	0.030	1.00	0.063	0.005	0.026
0.270	1.01	0.065	0.005	0.030	0.99	0.061	0.005	0.027
0.202	1.01	0.067	0.005	0.034	0.99	0.063	0.004	0.029
0.135	1.02	0.067	0.004	0.037	0.99	0.065	0.004	0.030
0.067	1.01	0.065	0.007	0.035	0.98	0.064	0.005	0.031
0.000	1.01	0.067	0.006	0.035	0.98	0.063	0.006	0.032

Unweighted Data

	Re = 57,400				Re = 110,000			
r/(D/2)	U/Ub	u'/Ub	V/Ub	v'/Ub	U/Ub	u'/Ub	V/Ub	v'/Ub
0.967	0.98	0.101	0.113	0.105	1.02	0.080	0.106	0.087
0.945	0.99	0.081	0.056	0.093	1.02	0.070	0.076	0.086
0.877	1.00	0.067	-0.004	0.080	1.02	0.070	-0.030	0.078
0.810	1.00	0.061	-0.043	0.053	1.00	0.064	-0.058	0.058
0.742	0.99	0.060	-0.032	0.048	1.00	0.059	-0.039	0.054
0.675	0.99	0.059	-0.022	0.047	0.99	0.059	-0.019	0.050
0.607	0.99	0.060	-0.011	0.049	0.99	0.058	-0.009	0.052
0.540	1.00	0.063	-0.003	0.048	1.00	0.062	-0.002	0.048
0.472	1.01	0.062	0.000	0.049	1.00	0.061	0.006	0.050
0.405	1.00	0.067	0.004	0.051	1.00	0.061	0.008	0.052
0.337	1.01	0.066	0.010	0.049	1.00	0.063	0.010	0.051
0.270	1.01	0.065	0.005	0.061	0.99	0.061	0.011	0.053
0.202	1.01	0.067	0.010	0.068	0.99	0.063	0.008	0.057
0.135	1.02	0.067	0.006	0.076	0.98	0.066	0.006	0.062
0.067	1.01	0.066	0.011	0.068	0.99	0.064	0.011	0.062
0.000	1.01	0.067	0.012	0.067	0.99	0.062	0.012	0.060

x/D = +1

Weighted Data

	Re = 57,400				Re = 110,000			
r/(D/2)	U/Ub	u'/Ub	V/Ub	v'/Ub	U/Ub	u'/Ub	V/Ub	v'/Ub
0.967	0.94	0.105	0.028	0.046	0.96	0.138	0.026	0.049
0.945	0.98	0.100	0.024	0.048	0.98	0.084	0.018	0.041
0.877	1.02	0.104	0.006	0.032	0.99	0.082	0.004	0.027
0.810	1.01	0.084	0.001	0.028	1.00	0.061	-0.010	0.030
0.742	1.03	0.067	-0.002	0.026	1.00	0.056	-0.011	0.028
0.675	1.02	0.074	-0.001	0.026	0.98	0.056	-0.003	0.021
0.607	1.03	0.067	0.002	0.025	0.99	0.054	-0.003	0.021
0.540	1.04	0.058	0.007	0.027	1.00	0.056	0.000	0.022
0.472	1.04	0.059	0.008	0.029	1.00	0.057	0.004	0.022
0.405	1.05	0.062	0.007	0.031	0.99	0.059	0.005	0.023
0.337	1.05	0.062	0.007	0.030	0.99	0.061	0.005	0.026
0.270	1.04	0.062	0.008	0.030	0.99	0.061	0.007	0.027
0.202	1.04	0.062	0.008	0.031	1.00	0.062	0.008	0.029
0.135	1.05	0.064	0.009	0.031	1.00	0.063	0.007	0.028
0.067	1.05	0.064	-----	-----	1.00	0.062	0.009	0.030
0.000	1.05	0.064	-----	-----	1.00	0.062	0.007	0.030

Unweighted Data

	Re = 57,400				Re = 110,000			
r/(D/2)	U/Ub	u'/Ub	V/Ub	v'/Ub	U/Ub	u'/Ub	V/Ub	v'/Ub
0.967	0.98	0.113	0.072	0.072	0.98	0.150	0.081	0.075
0.945	0.99	0.130	0.074	0.077	1.00	0.091	0.065	0.070
0.877	1.02	0.119	0.020	0.058	1.00	0.090	0.017	0.056
0.810	1.02	0.094	0.002	0.052	1.00	0.061	-0.033	0.051
0.742	1.02	0.080	-0.008	0.047	0.98	0.055	-0.039	0.045
0.675	1.02	0.093	-0.007	0.060	0.99	0.055	-0.013	0.042
0.607	1.03	0.081	0.004	0.045	0.99	0.055	-0.014	0.044
0.540	1.04	0.058	0.016	0.053	1.00	0.055	-0.003	0.041
0.472	1.05	0.059	0.018	0.054	1.00	0.056	0.011	0.042
0.405	1.05	0.061	0.014	0.063	1.00	0.058	0.014	0.043
0.337	1.05	0.062	0.017	0.057	0.99	0.060	0.015	0.051
0.270	1.05	0.061	0.020	0.050	0.99	0.060	0.021	0.050
0.202	1.05	0.062	0.019	0.054	1.00	0.061	0.023	0.051
0.135	1.05	0.064	0.021	0.058	1.00	0.062	0.021	0.053
0.067	1.05	0.064	-----	-----	1.00	0.062	0.026	0.054
0.000	1.05	0.063	-----	-----	1.01	0.062	0.029	0.056

x/D = +2

Weighted Data

	Re = 57,400				Re = 110,000			
r/(D/2)	U/Ub	u'/Ub	V/Ub	v'/Ub	U/Ub	u'/Ub	V/Ub	v'/Ub
0.967	0.86	0.132	0.020	0.040	0.93	0.103	0.014	0.037
0.945	0.92	0.098	0.018	0.036	0.95	0.082	0.010	0.033
0.877	1.01	0.066	0.010	0.024	1.02	0.063	0.006	0.025
0.810	1.03	0.052	0.005	0.025	1.01	0.057	-0.001	0.021
0.742	1.02	0.052	0.004	0.024	0.99	0.052	-0.002	0.020
0.675	1.02	0.049	0.003	0.022	0.99	0.052	-0.002	0.021
0.607	1.02	0.050	0.003	0.024	1.00	0.055	0.001	0.021
0.540	1.02	0.053	0.005	0.028	1.01	0.056	0.003	0.022
0.472	1.02	0.056	0.007	0.029	1.01	0.058	0.005	0.023
0.405	1.03	0.058	0.008	0.029	1.01	0.060	0.008	0.025
0.337	1.03	0.060	0.009	0.031	1.01	0.060	0.008	0.027
0.270	1.03	0.061	0.010	0.032	1.01	0.062	0.009	0.030
0.202	1.04	0.062	0.008	0.030	1.02	0.064	0.011	0.032
0.135	1.04	0.063	0.010	0.032	1.01	0.062	0.010	0.031
0.067	1.03	0.063	0.014	0.034	1.01	0.062	0.010	0.031
0.000	1.05	0.062	0.012	0.032	1.01	0.062	0.007	0.029

Unweighted Data

	Re = 57,400				Re = 110,000			
r/(D/2)	U/Ub	u'/Ub	V/Ub	v'/Ub	U/Ub	u'/Ub	V/Ub	v'/Ub
0.967	0.88	0.122	0.056	0.063	0.94	0.098	0.053	0.064
0.945	0.93	0.095	0.048	0.056	0.98	0.075	0.040	0.065
0.877	1.01	0.066	0.026	0.037	1.02	0.063	0.025	0.050
0.810	1.03	0.052	0.016	0.043	1.01	0.057	-0.004	0.041
0.742	1.02	0.053	0.010	0.041	1.00	0.053	-0.007	0.039
0.675	1.02	0.049	0.006	0.039	0.99	0.052	-0.008	0.040
0.607	1.02	0.050	0.005	0.041	1.00	0.055	0.000	0.041
0.540	1.02	0.053	0.012	0.052	1.01	0.055	0.008	0.041
0.472	1.02	0.057	0.018	0.051	1.02	0.058	0.011	0.041
0.405	1.04	0.058	0.020	0.052	1.02	0.060	0.024	0.046
0.337	1.04	0.060	0.021	0.067	1.01	0.060	0.024	0.050
0.270	1.04	0.061	0.024	0.065	1.02	0.062	0.030	0.052
0.202	1.04	0.062	0.019	0.061	1.02	0.064	0.033	0.058
0.135	1.04	0.064	0.026	0.054	1.02	0.062	0.032	0.054
0.067	1.03	0.063	0.034	0.056	1.01	0.062	0.032	0.054
0.000	1.05	0.061	0.035	0.052	1.02	0.062	0.026	0.054

x/D = +3

Weighted Data

	Re = 57,400				Re = 110,000			
r/(D/2)	U/Ub	u'/Ub	V/Ub	v'/Ub	U/Ub	u'/Ub	V/Ub	v'/Ub
0.967	0.93	0.076	0.015	0.039	1.00	0.073	0.002	0.031
0.945	0.95	0.069	0.017	0.039	1.02	0.067	0.005	0.025
0.877	0.98	0.053	0.011	0.030	1.02	0.057	0.002	0.023
0.810	1.00	0.048	0.005	0.026	1.01	0.055	-0.001	0.023
0.742	1.00	0.046	0.005	0.024	1.02	0.053	-0.001	0.021
0.675	1.02	0.052	0.005	0.024	1.03	0.057	0.000	0.021
0.607	1.02	0.052	0.003	0.024	----	-----	0.002	0.022
0.540	1.02	0.055	0.004	0.025	1.03	0.058	0.004	0.023
0.472	1.02	0.057	0.003	0.027	----	-----	0.007	0.026
0.405	1.02	0.061	0.004	0.027	1.04	0.060	0.009	0.028
0.337	1.02	0.065	0.006	0.029	1.04	0.065	0.011	0.031
0.270	1.02	0.068	0.007	0.030	1.04	0.068	0.012	0.031
0.202	1.03	0.067	0.008	0.031	1.04	0.068	0.013	0.033
0.135	1.02	0.068	0.008	0.031	1.03	0.068	0.013	0.033
0.067	1.02	0.068	0.007	0.031	1.02	0.068	0.010	0.032
0.000	1.02	0.067	0.008	0.031	1.02	0.071	0.009	0.031

Unweighted Data

	Re = 57,400				Re = 110,000			
r/(D/2)	U/Ub	u'/Ub	V/Ub	v'/Ub	U/Ub	u'/Ub	V/Ub	v'/Ub
0.967	0.94	0.074	0.045	0.064	1.01	0.072	0.030	0.063
0.945	0.95	0.067	0.048	0.061	1.02	0.069	0.019	0.052
0.877	0.99	0.053	0.033	0.049	1.02	0.058	0.002	0.048
0.810	1.00	0.048	0.015	0.045	1.02	0.056	-0.006	0.048
0.742	1.00	0.047	0.013	0.041	1.02	0.053	-0.004	0.041
0.675	1.01	0.049	0.014	0.040	1.04	0.057	0.000	0.044
0.607	1.02	0.052	0.006	0.041	----	-----	0.007	0.043
0.540	1.02	0.055	0.011	0.044	1.04	0.058	0.014	0.047
0.472	1.02	0.057	0.008	0.047	----	-----	0.023	0.048
0.405	1.02	0.061	0.011	0.048	1.04	0.060	0.030	0.052
0.337	1.02	0.064	0.014	0.053	1.04	0.064	0.037	0.054
0.270	1.02	0.067	0.018	0.052	1.04	0.068	0.039	0.055
0.202	1.03	0.066	0.022	0.053	1.04	0.068	0.042	0.054
0.135	1.03	0.067	0.022	0.052	1.04	0.068	0.042	0.059
0.067	1.03	0.066	0.020	0.054	1.03	0.068	0.037	0.060
0.000	1.03	0.067	0.022	0.052	1.03	0.070	0.029	0.060

x/D = +4

Weighted Data

	Re = 57,400				Re = 110,000			
r/(D/2)	U/Ub	u'/Ub	V/Ub	v'/Ub	U/Ub	u'/Ub	V/Ub	v'/Ub
0.967	0.93	0.105	0.010	0.037	0.94	0.084	0.004	0.029
0.945	0.98	0.081	0.010	0.036	0.98	0.078	0.006	0.031
0.877	1.02	0.071	0.006	0.027	1.01	0.062	0.003	0.023
0.810	1.05	0.064	0.003	0.024	1.01	0.060	0.000	0.020
0.742	1.04	0.067	0.002	0.022	1.01	0.053	0.000	0.020
0.675	1.03	0.057	-0.001	0.021	1.02	0.054	-0.001	0.020
0.607	1.05	0.057	0.002	0.022	1.01	0.062	-0.008	0.020
0.540	1.05	0.061	0.002	0.023	1.02	0.062	0.002	0.022
0.472	1.06	0.063	0.003	0.025	1.04	0.063	0.004	0.023
0.405	1.07	0.072	0.005	0.027	1.05	0.067	0.005	0.024
0.337	1.07	0.071	0.005	0.028	1.04	0.069	0.006	0.025
0.270	1.07	0.075	0.007	0.029	1.03	0.071	0.006	0.025
0.202	1.07	0.078	0.007	0.030	1.04	0.070	0.008	0.027
0.135	1.06	0.080	0.007	0.030	1.04	0.073	0.008	0.030
0.067	1.06	0.080	0.010	0.031	1.04	0.072	0.009	0.030
0.000	1.06	0.081	0.010	0.031	1.04	0.073	0.009	0.032

Unweighted Data

	Re = 57,400				Re = 110,000			
r/(D/2)	U/Ub	u'/Ub	V/Ub	v'/Ub	U/Ub	u'/Ub	V/Ub	v'/Ub
0.967	0.95	0.118	0.029	0.065	0.95	0.083	0.021	0.063
0.945	0.98	0.097	0.031	0.066	0.98	0.079	0.025	0.064
0.877	1.04	0.076	0.017	0.049	1.01	0.063	0.013	0.049
0.810	1.05	0.083	0.009	0.042	1.01	0.062	0.003	0.040
0.742	1.05	0.081	0.006	0.043	1.01	0.054	0.000	0.038
0.675	1.04	0.064	-0.001	0.037	1.02	0.054	-0.004	0.039
0.607	1.05	0.057	0.000	0.039	1.02	0.057	-0.002	0.040
0.540	1.05	0.061	0.000	0.041	1.03	0.062	0.006	0.042
0.472	1.06	0.064	0.001	0.045	1.04	0.062	0.012	0.044
0.405	1.08	0.070	0.011	0.047	1.04	0.063	0.016	0.046
0.337	1.08	0.070	0.012	0.050	1.05	0.066	0.020	0.047
0.270	1.08	0.074	0.019	0.051	1.04	0.070	0.021	0.048
0.202	1.07	0.076	0.019	0.052	1.04	0.070	0.025	0.050
0.135	1.06	0.078	0.020	0.054	1.04	0.072	0.027	0.054
0.067	1.07	0.078	0.022	0.069	1.04	0.071	0.031	0.054
0.000	1.07	0.078	0.027	0.052	1.04	0.072	0.035	0.058

x/D = +5

Weighted Data

	Re = 57,400				Re = 110,000			
r/(D/2)	U/Ub	u'/Ub	V/Ub	v'/Ub	U/Ub	u'/Ub	V/Ub	v'/Ub
0.967	0.89	0.131	0.009	0.035	0.89	0.104	0.003	0.026
0.945	0.92	0.105	0.007	0.032	0.93	0.097	0.002	0.025
0.877	1.00	0.087	0.005	0.027	1.00	0.068	0.002	0.022
0.810	1.05	0.071	0.005	0.023	1.01	0.064	0.000	0.020
0.742	1.05	0.054	0.003	0.021	1.02	0.058	0.001	0.020
0.675	1.05	0.055	0.004	0.022	1.02	0.053	0.003	0.022
0.607	1.05	0.060	0.004	0.023	1.03	0.060	0.002	0.022
0.540	1.06	0.065	0.003	0.025	1.03	0.064	0.004	0.023
0.472	1.06	0.070	0.006	0.027	1.04	0.066	0.006	0.027
0.405	1.07	0.074	0.008	0.029	1.04	0.068	0.008	0.028
0.337	1.07	0.078	0.011	0.034	1.05	0.074	0.009	0.028
0.270	1.07	0.088	0.008	0.031	1.04	0.079	0.009	0.030
0.202	1.07	0.088	0.011	0.033	1.05	0.077	0.011	0.032
0.135	1.07	0.089	0.012	0.034	1.05	0.080	0.012	0.034
0.067	1.08	0.090	0.012	0.033	1.05	0.082	0.012	0.033
0.000	1.08	0.090	0.013	0.033	1.06	0.079	0.010	0.031

Unweighted Data

	Re = 57,400				Re = 110,000			
r/(D/2)	U/Ub	u'/Ub	V/Ub	v'/Ub	U/Ub	u'/Ub	V/Ub	v'/Ub
0.967	0.89	0.131	0.028	0.064	0.90	0.100	0.010	0.053
0.945	0.92	0.118	0.021	0.058	0.94	0.087	0.009	0.052
0.877	1.01	0.102	0.015	0.047	1.00	0.068	0.007	0.044
0.810	1.05	0.090	0.012	0.040	1.02	0.066	0.001	0.040
0.742	1.05	0.053	0.008	0.038	1.02	0.060	0.001	0.039
0.675	1.05	0.055	0.008	0.038	1.02	0.053	0.008	0.042
0.607	1.06	0.060	0.007	0.041	1.03	0.059	0.007	0.043
0.540	1.07	0.064	0.006	0.045	1.04	0.063	0.014	0.046
0.472	1.07	0.069	0.013	0.049	1.05	0.065	0.020	0.051
0.405	1.07	0.074	0.021	0.050	1.05	0.068	0.026	0.053
0.337	1.08	0.077	0.030	0.056	1.05	0.072	0.028	0.053
0.270	1.08	0.085	0.023	0.056	1.05	0.077	0.034	0.054
0.202	1.08	0.086	0.029	0.056	1.06	0.076	0.035	0.057
0.135	1.07	0.086	0.031	0.058	1.05	0.079	0.038	0.067
0.067	1.09	0.088	0.032	0.055	1.06	0.080	0.035	0.057
0.000	1.09	0.088	0.035	0.055	1.06	0.077	0.037	0.058

This report was done with support from the Department of Energy. Any conclusions or opinions expressed in this report represent solely those of the author(s) and not necessarily those of The Regents of the University of California, the Lawrence Berkeley Laboratory or the Department of Energy.

Reference to a company or product name does not imply approval or recommendation of the product by the University of California or the U.S. Department of Energy to the exclusion of others that may be suitable.

TECHNICAL INFORMATION DEPARTMENT
LAWRENCE BERKELEY LABORATORY
UNIVERSITY OF CALIFORNIA
BERKELEY, CALIFORNIA 94720